

Large- N spacetime reduction and the sign and silver-blaze problems of dense QCD

Barak Bringoltz

Department of Physics, University of Washington, Seattle, WA 98195-1560, USA

and

Kavli Institute for Theoretical Physics China, CAS, Beijing 100190, China

We study the spacetime-reduced (Eguchi-Kawai) version of large- N QCD with nonzero chemical potential. We explore a method to suppress the sign fluctuations of the Dirac determinant in the hadronic phase; the method employs a re-summation of gauge configurations that are related to each other by center transformations. We numerically test this method in two dimensions, and find that it successfully solves the silver-blaze problem. We analyze the system further, and measure its free energy F , the average phase θ of its Dirac determinant, and its chiral condensate $\langle \bar{\psi}\psi \rangle$. We show that F and $\langle \bar{\psi}\psi \rangle$ are independent of μ in the hadronic phase but that, as chiral perturbation theory predicts, the quenched chiral condensate drops from its $\mu = 0$ value when $\mu \sim (\text{pion mass})/2$. Finally, we find that the distribution of θ qualitatively agrees with further, more recent, predictions from chiral perturbation theory.

I. INTRODUCTION

It is of great interest to calculate properties of four dimensional QCD at low temperatures and large, but not asymptotic, chemical potentials. Due to the ‘sign problem’ that inflicts euclidean lattice Monte-Carlo simulations such calculations seem currently unrealistic [1] (for recent progress in this see Ref. [2]). Specifically, the fluctuations in the phase θ of the Dirac operator’s determinant, which become particularly strong once the chemical potential μ grows beyond half the pion mass $m_\pi/2$, cause the simulations to fail. At a first glance this seems surprising because, at least for low temperatures $T \ll \Lambda_{\text{QCD}}$, one expects physics to depend on μ only once $\mu \gtrsim m_B/3$, with m_B the lightest baryon mass. Thus, for $m_\pi/2 \leq \mu \leq m_B/3$, physical observables are approximately independent of μ but θ is strongly oscillating. The apparent tension between these two facts was termed the ‘silver-blaze’ problem [3] and for small μ it can be studied with chiral perturbation theory [4]. The sign and silver blaze problems were also recently studied in scalar field theory using complex Langevin dynamics [5] and in fermionic theories with four-fermi interactions [6].

In this paper we analyze various aspects of the QCD sign problem. In particular, we ask how the sign problem behaves once we project the Dirac determinant to be neutral with respect to the Z_N center symmetry of the $SU(N)$ group. Our current paper is not the first to discuss this ‘ Z_N -averaging’ — see for example Refs. [8] — but we are not aware of studies that explicitly checked its effect on the sign fluctuations of the determinant in the confined phase of QCD.

Our modest computational resources lead us to approach the problem in its large- N ‘t Hooft limit and to utilize the space-time reduction of the planar theory. This reduction in degrees of freedom was discovered by Eguchi and Kawai in the seminal Ref. [9] whose content is the following: under certain conditions, infinite-volume lattice large- N QCD is equivalent, on all distance scales, and in certain sectors of its spectrum, to its ‘volume-reduced’ version. The latter is nothing but lattice QCD defined on a single lattice site.

The simplest implementation of the Eguchi-Kawai (EK) equivalence works only in two euclidean dimensions [10, 11], while in four dimensions, some extensions of the original EK prescription, like those of Ref. [12, 13], are expected to be successful. The numerical work in-

volved in using these extended prescriptions is comparably demanding, and their applicability is still being tested numerically [14, 15]. These facts lead us to focus on the two-dimensional system in this paper. Provided that the constructions of Refs. [12, 13] survive their numerical tests, we do not see any obvious numerical or conceptual difficulties in extending the present approach to four dimensions.

Below is the outline of our paper. We begin in Section II by reminding the reader what are the validity conditions of the EK equivalence and discuss what they imply for our numerical calculations. We then present the construction of the two-dimensional EK theory in Section III, and discuss how we simulate it and which observables we measure. We formulate Z_N -averaging in Section IV. Then, in Section V, we discuss the connection of the sign and silver-blaze problems to the signal to noise ratio (SNR) of physical observables calculated with a Monte-Carlo simulation, and the way Z_N averaging can potentially solve these problems. In Section VI we present our numerical study of the sign problem and show the average sign of the determinant as a function of μ . The tests of Z_N -averaging are presented in Section VII. We then show results from measurements of various physical observables in Section VIII, and in Section IX we present the distributions of θ as a function of μ , and the way the eigenvalues of the Dirac operator scatter in the complex plane for different values of μ . In Section X we summarize our study.

II. EGUCHI-KAWAI SPACE-TIME REDUCTION AT NONZERO DENSITY

There are two issues one should be aware of when one studies nonzero density with space-time reduction. We discuss these issues in Sections II A and II B, where we show that the method of EK space-time reduction can be used only within the hadronic phase. Despite that, this method is useful to understand the silver blaze and sign problems of QCD at nonzero μ , and we emphasize this point in Section II C.

A. The importance of translation symmetry

In Ref. [16] we studied the space-time reduction of large- N QCD in the presence of baryons. To have full analytic control we focused there on the two-dimensional version of QCD – the ‘t Hooft model. We found results which are consistent with the general validity conditions that non-perturbative large- N equivalences require. Specifically, we saw that the main validity condition for volume reduction (or the ‘Eguchi-Kawai equivalence’) in our context is that translation symmetry is intact in the infinite-volume field theory.¹ To understand this recall that the EK theory is the single-site version of QCD. Thus, it is a projection of QCD that removes degrees of freedom with nonzero momentum. As such, it is clear that using the EK equivalence does not make sense when the vacuum of QCD spontaneously breaks translation invariance and is characterized by condensates which carry nonzero momentum. The question of whether translations are a symmetry of the QCD ground state at nonzero μ is a dynamical one, and in Ref. [17] we showed that in two dimensions, for any quark mass, and for a single flavor, this symmetry breaks spontaneously for $\mu > m_B/N$ (for earlier results concerning only the chiral limit see Ref. [18]). Simple arguments lead one to expect a similar phenomenon in higher dimensions (see discussion in section IV of Ref. [17]). This means that the single site theory that we study in the current paper is equivalent to the infinite-volume field theory throughout the hadronic phase which, in two dimensions and in the single flavor case, is bounded by $\mu \leq m_B/N$. Beyond that point the theory we study here can be thought of as a complicated matrix model.

B. Implications of lattice saturation

As any lattice field theory, volume-reduced QCD can be expected to be influenced by lattice artifacts at sufficiently large values of μ . In particular, for lattice spacing a and chemical potential $\mu \sim O(1/a)$, the density is at the cutoff scale, and the lattice is saturated with baryons – there is an $O(1)$ number of baryons per site. This regime, in which the Pauli

¹ Another condition is that the Z_N center symmetry of the theory is intact, but this is dictated by the leading gluon dynamics and not by the fermions.

exclusion on each site is saturated or nearly saturated, is usually referred to as the lattice saturation regime and is governed by lattice artifacts.

What does the saturation phenomenon imply on a single-site theory? In $d + 1$ dimensions the spatial volume V of the single-site theory is a^d , and as long as μ is smaller than a critical value μ_c , there are no baryons in the vacuum (as mentioned above, for $d = 1$ and with a single flavor, baryons repel and $\mu_c = m_B/N$ [17, 19]). But when $\mu > \mu_c$ the hadronic phase makes way to a phase that accommodates baryons, and the baryon number B is then at least 1. Importantly, this makes the baryon density, B/V , of $O(1/a^d)$ and so at the cutoff scale.

Therefore, we see that we cannot accommodate physical *nonzero* densities on a single site: when the baryon number is nonzero, it is at least one, the density of the single-site theory is at the cutoff scale.

C. Usefulness of space-time reduction at nonzero μ .

At this point an obvious question comes to mind — what is the usefulness of the EK single-site theory at $\mu > 0$ and why do we wish to study it in this paper? The answer is that we wish to understand the sign and silver blaze problem of the hadronic phase. In that phase μ is nonzero, but the density *is* zero and so we can use the EK theory to analyze the theory there.

Also, despite the fact that in the saturation regime (outside the hadronic phase), the EK theory is not equivalent to the field theory, we can still ask how the EK model behaves there, and see whether we can learn something about the general properties of the saturation regime (as we alluded to above, this regime appears also in the standard, infinite-volume, ‘non-reduced’ lattice field theory).

III. LATTICE DETAILS OF THE EGUCHI-KAWAI THEORY AT NONZERO μ : THE ACTION AND THE SIMULATION ALGORITHM

The EK theory or ‘volume-reduced QCD’ is a lattice gauge theory defined on a single lattice site. Since our numerical efforts are focused on two dimensions, we define below the

construction of the EK theory only in this case.

A. Definition of path integral

The path integral is

$$Z = \int DU \int D\psi D\bar{\psi} \exp(S_{\text{YM}} + S_F), \quad (3.1)$$

$$S_{\text{YM}} = 2Nb \operatorname{Re} \operatorname{Tr} (U_1 U_2 U_1^\dagger U_2^\dagger), \quad (3.2)$$

$$S_{\text{Dirac}} = \bar{\psi} D \psi, \quad (3.3)$$

$$D = \hat{m} + \frac{1}{2}\gamma_1 (U_1 e^{\hat{\mu}} - e^{-\hat{\mu}} U_1^\dagger) + \frac{1}{2}\gamma_2 (U_2 - U_2^\dagger), \quad (3.4)$$

Here $U_{1,2}$ are $SU(N)$ matrices and $DU = dU_1 dU_2$ with $dU_{1,2}$, the Haar measure on $SU(N)$. ψ is a two dimensional Dirac spinor of the ‘naive’ fermion type and it transforms in the fundamental representation of the gauge group. Thus, it corresponds to $4 \times N_f$ Dirac fermions in the continuum. The $2N_f N \times 2N_f N$ matrix D is the euclidean Dirac operator of a lattice gauge theory on a single site. The quark mass m and chemical potentials μ are related to their dimensionless lattice quantities \hat{m} and $\hat{\mu}$ in the usual way by the lattice spacing a . In two dimensions the gauge coupling g has dimensions of mass and the standard dimensionless lattice coupling β is defined by

$$\beta = \frac{2N}{a^2 g^2}. \quad (3.5)$$

In the ‘t Hooft limit g^2 scales like $O(N^{-1})$ and so it is useful to define a new lattice coupling $b = \beta/(2N^2)$ that scales like $O(N^0)$ in the large- N limit – this is the coupling that appears in Eq. (3.2). In terms of the dimensionful ‘t Hooft coupling $\lambda = g^2 N$, the coupling b is given by

$$b = \frac{1}{a^2 \lambda}. \quad (3.6)$$

All dimensionful quantities like the quark mass m and the baryon chemical potential μ will be fixed in units of λ when we take the continuum limit $b \rightarrow \infty$. Also, to make a connection with Ref. [20], we define the parameter γ that controls the quark mass

$$\gamma = \pi \frac{m^2}{\lambda}. \quad (3.7)$$

In terms of b and γ the lattice quantities are given by

$$\hat{m} \equiv am = \frac{m}{\sqrt{\lambda}} \frac{1}{\sqrt{b}} = \sqrt{\frac{\gamma}{\pi b}}, \quad (3.8)$$

$$\hat{\mu} \equiv a\mu = \frac{\mu}{\sqrt{\lambda}} \frac{1}{\sqrt{b}}. \quad (3.9)$$

It is useful to note the following results on the spectrum of the 't Hooft model in the large- N limit: The pion mass at zero chemical potential for small and large values of γ is given by (see Ref. [20])

$$\frac{m_\pi}{\sqrt{\lambda}} \simeq \begin{cases} 1.08 \gamma^{1/4} + O(\gamma^{1/2}) & \gamma \ll 1, \\ 1.13 \gamma^{1/2} + O(\gamma^{-2/3}) & \gamma \gg 1, \end{cases} \quad (3.10)$$

which is expected to hold for any number of flavors N_f that obeys $N_f \ll N$. Next, the lightest excitation with a nonzero baryon number *in the single-flavor case* is the baryon whose mass in the chiral limit is [19]

$$\frac{m_B}{N} = \frac{4}{\pi} \times \frac{m_\pi}{2}. \quad (3.11)$$

Indeed, in two dimensions, both m_π and m_B vanish for massless quarks! For a non-zero quark mass, however, $m_B/N > m_\pi/2$ and we have the intermediate range, $m_\pi/2 \lesssim \mu \lesssim m_B/N$, where the theory has the same properties as those at $\mu = 0$, but where the sign fluctuations are strong — just like in the case of physical four dimensional QCD.

The most recent calculation of the m_B/N in $1 + 1$ dimensions (for $N_f = 1$), away from the chiral limit, was done in Ref. [17]. The previous study in Ref. [19] had certain ingredients missing, whose effect was calculated in Ref. [17], and was found to be small. In any event, using the methods of Ref. [17], we evaluated the baryon mass for the quark mass studied in the current paper and we find²

$$\frac{m_B}{N\sqrt{\lambda}} \simeq 0.758 \quad \text{at} \quad \gamma = 1. \quad (3.12)$$

We note that both the estimates for m_B in Eqs. (3.12) and (3.11) are for $N_f = 1$ and we are not aware of any extensions to general N_f . Since we define the EK theory with naive fermions, for sufficiently small lattice spacings we actually have four physical Dirac fermions. In the

² This estimate was obtained in the Hamiltonian formalism at a spatial lattice spacing of $a\sqrt{\lambda} \simeq 0.31$. The lattice spacing corrections are expected to be small for this value of a [17].

absence of any estimates for the baryon mass in the four-flavor case, we proceed by assuming that the N_f dependence of m_B is weak.

B. Calculation strategy

Expectation values are measured with Monte-Carlo simulations that use the Yang-Mills action to generate gauge configurations. This means that $\langle \mathcal{O} \rangle$ is approximated by the sum over gauge configurations that represent the YM ensemble:

$$\langle \mathcal{O} \rangle \simeq \frac{1}{M} \sum_{c=1}^M \mathcal{O}_c. \quad (3.13)$$

Here M is the number of configurations. Our measurements can be therefore referred to as performed via ‘reweighting’ because we generate the gauge configurations with the YM action, and reweight in the fermion determinant.

This reweighting would not be necessary had we focused on $\mu = 0$ since the large- N theory is naturally quenched there (at least at nonzero quark mass); in practice this would be reflected in a Monte-Carlo by the fact that the ‘fermionic force’ in a Hybrid Monte-Carlo is $O(1/N)$ suppressed compared to the gluonic force. At $\mu > 0$, however, reweighting in the phase of the determinant is crucial (as our results would show).

By reweighting from the YM ensemble, we use the fact that the important gluonic configurations at large- N are chosen by the YM action, and that the fermions do not back-react to the gluons. This absence of back-reaction is characteristic of the large- N limit and can be justified in various approaches (like Hamiltonian coherent states) but we will not discuss this issue here (see instead the forthcoming Ref. [30]). We should note that the lack of back-reaction at large- N persists at nonzero μ , but that this does not mean that the quenched approximation should work there (despite the common lore, the quenched approximation is *not* equivalent to removing the back-reaction of quarks on gluons from QCD – more details will be given in Ref. [30]).

In the context of standard lattice QCD studies, the reweighting procedure is known to be highly susceptible to significant systematic errors when μ and the lattice volume are large enough [1]. These errors can be diminished, however, if one scales the number of sampled field

configurations *exponentially* in the size of the matrix D . In four dimensional 3-color QCD one has $\dim(D) = 12 \times (\text{lattice volume})$, and so going to the thermodynamic limit is not realistic with current computational power. Similarly, in our case we have $\dim(D) = 2 \times N$ and our computational resources allow us to study only $N \leq 60$.³

To simulate S_{YM} we used the heat-bath algorithm introduced in [21]. Measurements of fermionic quantities are typically separated by 100 – 1000 full updates of the model,⁴ and thus are expected to be uncorrelated. To check this we estimate errors with a jackknife procedure. Below we list the fermionic quantities that we measure for most values of b , N and μ .

- a. The fermionic contribution to the free energy, F . This was obtained from

$$F = \frac{1}{N} \log Z_{QCD} \equiv \frac{1}{N} \log \langle \det D(\mu) \rangle. \quad (3.14)$$

- b. The average sign of the determinant given by

$$\langle \cos(\theta) \rangle \equiv \left\langle \text{Re} \left(\frac{\det D(\mu)}{|\det D(\mu)|} \right) \right\rangle. \quad (3.15)$$

- c. The quenched quark condensate which we define to be

$$\langle \bar{\psi}\psi \rangle_{\text{quenched}} = \left\langle \text{tr} \left(D^{-1}(\mu) \right) \right\rangle. \quad (3.16)$$

- d. The physical unquenched quark condensate

$$\langle \bar{\psi}\psi \rangle_{\text{unquenched}} = \frac{\langle \text{tr} (D^{-1}(\mu)) \times \det D \rangle}{\langle \det D \rangle}. \quad (3.17)$$

- e. The distribution of the angles θ and α defined via

$$\det D = |\det D| e^{i\theta}, \quad (3.18)$$

$$\bar{\psi}\psi = |\bar{\psi}\psi| e^{i\alpha}. \quad (3.19)$$

³ Our errors modestly increase with N , and this is because we do not actually increase our statistical sample exponentially. Nevertheless, we find that $N = 40$ and 60 are already close enough to the large- N limit and in most cases have errors that are sufficiently small for our purposes. Indeed, this is how large- N reduction plays an important role in our study.

⁴ By ‘full update’ we mean updating all the $N(N-1)/2$ $SU(2)$ subgroups of each of the two matrices $U_{1,2}$.

f. The way the eigenvalues of D scatter in the complex plane.

Finally, for $\mu = 0$ and for each value of b and N we also measured the pion propagator of momentum q along the “2” direction using the Gross-Kitazawa momentum injection method [22] (that was also used in Ref. [23]). This means that we measure

$$G_\pi(q) = \left\langle \text{tr} \left(D^{-1}(U_2 e^{iq/2}) \gamma_5 D^{-1}(U_2 e^{-iq/2}) \gamma_5 \right) \right\rangle, \quad (3.20)$$

and extract the pion mass by measuring the effective mass m_{eff} defined by

$$m_{\text{eff}} = - \lim_{x \rightarrow \infty} \frac{\partial [\log (\text{Re} \int dq e^{iqx} G_\pi(q))] }{\partial x}. \quad (3.21)$$

We calculated these observables for chemical potentials in the range $\mu/\sqrt{\lambda} \in [0, 3]$. Throughout our calculation we fixed $\gamma = 1$ and so we expect $m_\pi/\sqrt{\lambda} \simeq 1.2$ from Eq. (3.10) and $m_\pi/\sqrt{\lambda} \simeq 1.5$ from the continuum extrapolations of the numerical results in [20]. We perform lattice simulations at $b = 0.6, 6.0, 10.0$. The number of field configurations that we used for each choice of N and b is given in Table I. We also list the pion mass in each case as measured from Eq. (3.21). For brevity, we set $\frac{1}{2}m_\pi/\sqrt{\lambda} = 0.65_{-0.05}^{+0.03}$ to encompass all the values of $m_\pi/2$ from Table I. We present the results of our study in the next sections.

The numerical routines we used were defined with double precision, and to check whether our calculations are sensitive to this (especially our evaluations of the determinants) we recalculated the free energies and average signs with quadruple precisions and confirmed that our results remained the same.

IV. DEFINITION OF Z_N -AVERAGING

In this section we define Z_N -averaging and briefly explain its logic. This averaging relies on the Z_N symmetry of the YM part of the action and of the Haar measure, and it is defined by the following prescription.

For each gauge configuration \mathcal{C} , characterized by the gauge fields (U_1, U_2) , perform the replacement

$$\mathcal{O}_\mathcal{C}(U_1, U_2) \rightarrow (\mathcal{O}_\mathcal{C})_Z \equiv \frac{1}{N^2} \sum_{k_1, k_2=1}^N \mathcal{O}_\mathcal{C} \left(U_1 e^{2\pi i k_1/N}, U_2 e^{2\pi i k_2/N} \right), \quad (4.1)$$

N	b	no. of configurations	$m_\pi/\sqrt{\lambda}$
	0.6	16000	$\lesssim 1.20$
10	6.0	20000	1.24(12)
	10.0	20000	1.24(13)
	0.6	12000	$\lesssim 1.24$
20	6.0	120000	1.25(5)
	10.0	120000	1.33(6)
	0.6	1000	$\lesssim 1.29$
40	6.0	105000	$\lesssim 1.23$
	10.0	101000	$\lesssim 1.40$
60	10.0	50000	–

TABLE I: Details of runs used to map the phase diagram in μ . The number of full model updates was of $O(10^6 - 10^7)$ depending on the value of N . Not all configurations were used to estimate the meson masses. The cases in which we only give an upper bound on m_π are those in which we did not observe the asymptotic mass plateau in the pion propagator. The reason for this is either that m_π was too large in lattice units, and so falls into the noise quickly (we saw this for $b = 0.60$), or that one needs to calculate the pion propagator at separations x which are too large for our resources to accommodate.

and only then average over the field configurations $U_{1,2}$. We distinguish between the results obtained with and without this Z_N -averaging by adding the subscript Z to the former, when necessary. In four dimensions Eq. (4.1) is generalized to have four sums over $k_{1,2,3,4} \in [1, N]$.

Let us explain the logic behind this proposal. We expect that the partition function will depend on μ in a very special way; for a $U(N)$ group there should be no μ -dependence since there are no gauge invariant charges that couple to μ . For an $SU(N)$ group, however, there *can* be μ -dependence, but only through the combination μN since the only gauge invariant excitations that couple to μ are baryons, and these have charges that are integer multiples of N .

How can we anticipate these results from the path integral in Eq. (3.1)? Expand $\det D$ in

Eq. (3.1) in the worldline approach [7]. It is then easy to see that the μ -dependence we discuss above arises because both the measure of the path integral and the YM action are symmetric under the center of the gauge group. Specifically, the μ dependence of the determinant comes in through terms of the form

$$e^{q\mu} \times \prod_i \left(\text{tr } U_1^{k_i} \right)^{p_i}, \quad \text{and} \quad e^{-q\mu} \times \left[\prod_i \left(\text{tr } U_1^{k'_i} \right)^{p'_i} \right]^\star, \quad (4.2)$$

with $q = \sum_i k_i p_i = \sum_i k'_i p'_i$, but the center symmetry allows $q = 0$ for $U(N)$ and $q/N =$ integer for $SU(N)$; Z_N -averaging enforces the center symmetry on each gauge configuration, and automatically makes the path integral depend on μ as prescribed above. In fact, since it is only U_1 that appears in Eq. (4.2), we can also try and do a partial Z_N averaging by re-summing gauge configurations that differ by a center transformation only in the time direction.

$$\mathcal{O}_C(U_1, U_2) \rightarrow (\mathcal{O}_C)_{Z\text{-partial}} \equiv \frac{1}{N} \sum_{k_1=1}^N \mathcal{O}_C(U_1 e^{2\pi i k_1/N}, U_2). \quad (4.3)$$

In our two-dimensional case this saves a factor of N in the measurements of observables (and N^{d-1} for d space-time dimensions). Numerically we see that, at least in the hadronic phase, such a partial averaging is almost as good as the full Z_N averaging (see Section VII), and so we use it when our resources are insufficient to perform the latter (for example when we calculate the unquenched quark condensates for $SU(40)$ or the average sign for $SU(60)$).

V. CAN Z_N AVERAGING SOLVE THE SILVER-BLAZE AND SIGN PROBLEMS?

As explained above, one reason that we expect Z_N averaging to be useful is that it makes the anticipated dependence of the partition function Z_{QCD} on μ manifest on a configuration-by-configuration basis — it is a noise reduction technique. To make this expectation more precise we need to discuss the source of the statistical noise in the calculation of Z_{QCD} for $\mu > 0$ (and its relation to the sign problem).⁵ We do so in Section V A, and then move on to Section V B where we discuss how such noise can be reduced when one uses Z_N averaging.

⁵ For a previous useful discussion on see Ref. [24].

A. The sign problem, the signal to noise ratio, and pion physics.

The sign problem and the signal to noise ratio (SNR) of observables in QCD are closely related. To show this, let us discuss the SNR of observables in a Monte-Carlo that generates gauge configurations for the ‘Phase-Quenched’ (PQ) ensemble. The measure of this ensemble is proportional to the absolute value of the Dirac determinant. Specifically, if we write

$$\det D = |\det D| e^{i\theta}, \quad (5.1)$$

then, when calculating the expectation value of an observable \mathcal{O} with gauge configurations of the PQ ensemble, one needs to treat the phase $e^{i\theta}$ as part of the observable. This means that the QCD average of \mathcal{O} becomes

$$\langle \mathcal{O} \rangle_{\text{QCD}} \equiv \frac{\langle \mathcal{O} e^{i\theta} \rangle_{\text{PQ}}}{\langle e^{i\theta} \rangle_{\text{PQ}}}. \quad (5.2)$$

It is useful to note that we can define the PQ average $\langle, \rangle_{\text{PQ}}$ through the Yang-Mills average $\langle, \rangle_{\text{YM}}$

$$\langle \mathcal{O} \rangle_{\text{PQ}} \equiv \frac{\langle \mathcal{O} |\det D| \rangle_{\text{YM}}}{\langle |\det D| \rangle_{\text{YM}}}. \quad (5.3)$$

From Eq. (5.2) we see that the SNR of any observable gets a contribution from the SNR of $\langle e^{i\theta} \rangle_{\text{PQ}} = \langle \cos \theta \rangle_{\text{PQ}}$ (here we assume charge conjugation). The SNR of $\langle \cos \theta \rangle_{\text{PQ}}$ is given by

$$\text{SNR}_{\cos \theta}^{\text{PQ}} \equiv \frac{(\langle \cos \theta \rangle_{\text{PQ}})^2}{\langle \cos^2 \theta \rangle_{\text{PQ}}}. \quad (5.4)$$

In terms of $\langle, \rangle_{\text{YM}}$, Eq. (5.4) becomes

$$\text{SNR}_{\cos \theta}^{\text{PQ}} \equiv \frac{(\langle \cos \theta | \det D | \rangle_{\text{YM}})^2}{\langle \cos^2 \theta | \det D | \rangle_{\text{YM}} \langle | \det D | \rangle_{\text{YM}}} = \frac{(\langle \det D \rangle_{\text{YM}})^2}{\langle \cos^2 \theta | \det D | \rangle_{\text{YM}} \langle | \det D | \rangle_{\text{YM}}}, \quad (5.5)$$

and it is now clear that if there is no sign problem, and $\cos \theta \approx 1$ for the majority of field configurations, then $\text{SNR}_{\cos \theta}^{\text{PQ}} \simeq 1$.

It is instructive to show how pion physics tends to appear when there is a sign problem. This can be seen by assuming that a sign problem makes $\cos^2 \theta \simeq \frac{1}{2}$ and turns Eq. (5.5) into

$$\text{SNR}_{\cos \theta}^{\text{PQ}} \simeq 2 \left(\frac{\langle \det D \rangle_{\text{YM}}}{\langle | \det D | \rangle_{\text{YM}}} \right)^2. \quad (5.6)$$

Now, for simplicity, consider the case of two degenerate flavors and note that

$$\text{SNR}_{\cos\theta}^{\text{PQ}} \simeq 2 \left(\frac{\langle \det D_1^2 \rangle_{\text{YM}}}{\langle |\det D_1|^2 \rangle_{\text{YM}}} \right)^2 = 2 e^{+2V/T(f_I - f_B)}. \quad (5.7)$$

Here D_1 is the Dirac operator of a single flavor and f_B and f_I are the free energy densities of two-flavor QCD in the presence of baryon number and isospin chemical potentials that are both equal to μ . To proceed, note that baryons do not contribute to f_B for $\mu \lesssim m_B/N$ (we always restrict to low temperatures) which gives

$$f_B(\mu) = f_B(0) \quad \text{for} \quad \mu < m_B/N. \quad (5.8)$$

In contrast, f_I changes when $\mu > m_\pi/2$ (the iso-spin system goes through pion condensation above this value of μ). These facts, together with $f_I \leq f_B$, which is true because $\langle |\det D_1^2| \rangle_{\text{YM}} \geq \langle \det D_1^2 \rangle_{\text{YM}}$, tell us that $\text{SNR}_{\cos\theta}^{\text{PQ}}$ is exponentially small in the four-volume V/T when

$$m_\pi/2 \leq \mu \lesssim m_B/N. \quad (5.9)$$

B. Two scenarios for the numerical cause of the sign problem and how Z_N averaging can solve it

We can understand the problem of the exponential suppression of $\text{SNR}_{\cos\theta}^{\text{PQ}}$ and the associated sign problem from the point of view of the worldline approach. In particular, these problems reflect sign fluctuations in $\det D$ that are caused by the contribution to $(\det D)$ from Polyakov loops that wrap around the temporal direction. From this point of view, there are two scenarios for the cause of the sign problem:

1. Scenario no. 1: The sign problem is caused by fluctuations of Polyakov loops that wrap the torus k times with $k/N \neq \text{integer}$.

Polyakov loops whose winding number around the temporal direction k is not an integer multiple of 3 (or N in $SU(N)$) are unphysical; by the center symmetry these nonzero N -ality worldlines have zero expectation value and so they do not contribute to the numerator of

Eq. (5.7). This is despite the fact that they appear in $\det D_1^2$ with enhancing fugacity factors of $e^{k\mu/T}$.

While the unphysical worldlines do not contribute to $\langle \det D_1^2 \rangle_{\text{YM}}$, they do contribute to its noise $\langle |\det D_1|^2 \rangle$ appearing in the denominator of Eq. (5.7); despite the fact that their magnitude can be small, their fugacity factors $e^{k\mu/T}$ can be large, and they can cause significant fluctuations in the overall fluctuating phase of the determinant. The magnitude squared of a k -worldline contribution to $\det D_1^2$ is a worldline configuration with k worldline-antiworldline pairs which can be interpreted as a worldline of k pions (this can be seen explicitly from the worldline expansion of the $|\det D_1|^2$). Therefore, this magnitude squared can be estimated by $e^{-km_\pi/T}$, and we can now anticipate that $\det D_1^2$ will have significant noise when $e^{k\mu/T} \times e^{-km_\pi/2T} \gg 1$ or when $\mu > m_\pi/2$, as we saw in Eq. (5.9).⁶

If the scenario we describe above is the one causing the sign problem then it is an optimistic scenario: worldlines that wrap the euclidean time torus k times with $k/N \neq \text{integer}$ can be removed from the noise on a configuration-by-configuration basis using Z_N averaging. This would solve the silver-blaze problem since it would remove the phase fluctuations of the Dirac determinant in the hadronic phase.

Importantly, however, our focus on the unphysical worldlines in the current scenario assumes that the physical, ‘baryonic’, worldlines with $k/N = \text{integer}$, are suppressed on a configuration-by-configuration basis (assuming, for example, that they are weighted by $e^{-km_B/T}$). If that is the case then the only sign fluctuations that would survive Z_N averaging would occur when the baryonic worldlines contribute to $\langle \det D_1^2 \rangle$, i.e. when $\mu > m_B/N$. In the next scenario below we ask what happens if this is *not* the case.

2. Scenario no. 2: The sign problem is caused by Polyakov loops that also have $k/N = \text{integer}$.

Unfortunately, the physical, ‘baryonic’, worldlines, for which k is an integer multiple of N (and therefore are insensitive to Z_N averaging), can have a sizable contribution to the sign and

⁶ In principle we should replace km_π by the free energy of a system with isospin number equal to k , but the binding energy of k pions is suppressed at large- N .

SNR problems even at small μ . Naively one might think that these worldlines are suppressed so long as $\mu \lesssim m_B/N$ (see end of previous section) but this is not necessarily correct. To see why, let us focus on the single-baryon contribution to $(\det D)$, and denote it by $(\det D)_{B=1}$. The latter reflects the contributions of all worldlines that wrap the euclidean circle N times and so it comes with a fugacity pre-factor of $e^{N\mu/T}$. Our main point here is that there is no a priori reason why these contributions should be suppressed by $e^{-m_B/T}$ on a configuration-by-configuration basis. Quite the contrary, it is possible that there are some gauge configurations where these contribution are of $O(e^{-Nm_\pi/2})$ — here we view the weight of a single quark line as the weight of half of a pion.⁷

Thus, we propose that $(\det D)_{B=1}$ evaluated on a single gauge configuration would have the following generic form reflecting the fact that its noise (or absolute value squared) has a combined origin of both a baryon-antibaryon pair or N pions.

$$(\det D)_{B=1} \approx e^{(N\mu - m_B)/T} + c \times e^{N(\mu - m_\pi/2)/T}. \quad (5.10)$$

Here the (generally complex) number c depends on the dynamical details of the theory and on a configuration-by-configuration basis can be of an $O(1)$ magnitude but strongly fluctuating. In particular, the fluctuations in c can average the second term in Eq. (5.10) to zero, such that the gauge-configuration average will make $\langle (\det D)_{B=1} \rangle$ (that determines the baryon mass) associated only with the N world-lines that bind into a baryon.

From Eq. (5.10) we see that if we send $T \rightarrow 0$, then the second term is the dominant one (since m_π is always smaller than $2m_B/N$). This means that when $\mu > m_\pi/2$ pions will proliferate in the noise of $\det D$ and there will be a severe sign problem. In contrast, if we keep T finite (but low), and if $|c|$ happens to be numerically very small, or more precisely if

$$|c| \ll e^{(N/2m_\pi - m_B)/T}, \quad (5.11)$$

then the pionic term can become irrelevant. In that case $(\det D)_{B=1}$ will be of the order of $e^{-m_B/T}$ for most of the gauge configurations, and all the μ dependence of $\det D$ will be

⁷ Indeed, the noise in the evaluation of $(\det D)_{B=1}$ is given by the magnitude squared of $(\det D)_{B=1}$, and can describe either a baryon-antibaryon pair or an N -pion system (both can be described by N worldline-antiworldlines pairs).

exponentially suppressed if $\mu < m_B/N$. Then $\det D$ will behave like it does at $\mu = 0$, i.e. there will be no sign problem.

It is Eq. (5.11) that determines whether Z_N averaging solves the sign problem or not. Similar arguments lead the search for optimized baryonic wave functions that couple minimally to pion physics, thus improving the signal to noise ratio of baryon correlation functions [26]. In that context, one searches for a ‘golden window’ in the euclidean time separation of baryonic correlators, where their SNR is not exponentially small. Here, Eq. (5.11) defines a golden window in the temperature T .

In the following sections we present results from numerical simulations, some of which done in order to determine whether Z_N averaging indeed removes the sign fluctuations in the hadronic phase and solves the associated silver-blaze problem. Put differently we aim to see whether it is scenario no. 1 or no. 2 that takes place in our system.

VI. RESULTS : THE SIGN PROBLEM

In this section we present the numerical analysis we performed for the averaged sign. We begin by presenting the way the average sign of $\det D$ behaves as a function of μ for $SU(40)$ and different values of b in Fig. 1. The vertical (gray) solid band in the figure denotes our estimate for $m_\pi/2 \approx 0.65\sqrt{\lambda}$ (see above). The dashed vertical (red) line denotes the baryon mass m_B (divided by N) for the single-flavor case. It is higher than $m_\pi/2$ by only about 16% (this proximity is special to $1 + 1$ dimensions). As we emphasize in Section II, the EK theory that we study is equivalent to the $2d$ gauge theory on an infinite volume *only* below m_B/N . We nevertheless present here (and below) the results for larger values of μ , since for these values of μ the model has a saturation behavior which is accompanied by an interesting behavior in the average sign. Specifically, from Eq. (3.4) we see that when the EK theory is saturated with baryons, it has no sign fluctuations because the $e^{\hat{\mu}}$ term governs the behavior of D and one has

$$D \sim U_1 e^{\hat{\mu}} \left(1 + O(e^{-\hat{\mu}}) \right). \quad (6.1)$$

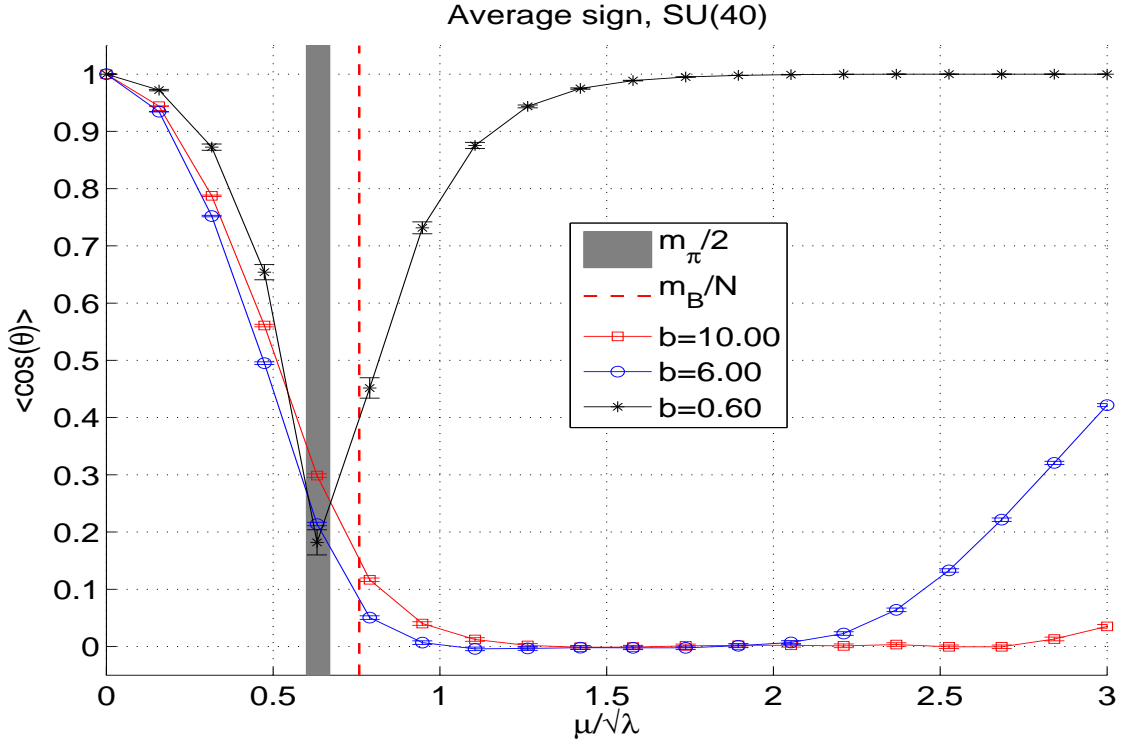


FIG. 1: The average sign, $\langle \cos(\theta) \rangle$ for $SU(40)$ and $b = 0.60, 6.00, 10.00$.

Since $U_1 \in SU(N)$ this means that

$$\det D \xrightarrow{\text{saturation}} e^{2N\hat{\mu}}, \quad (6.2)$$

and that $\langle \cos \theta \rangle \rightarrow 1$. Looking at Fig. 1, we see that this is happening at $\mu_{\text{saturation}}/\sqrt{\lambda} \simeq 1.5$ for $b = 0.60$, and starting to happen at $\mu_{\text{saturation}}/\sqrt{\lambda} \simeq 3.0$ for $b = 6.00$. The increase with b of $\mu_{\text{saturation}}$ is expected since in the continuum limit, $b \rightarrow \infty$, the saturation goes away completely (recall that this saturation reflects the fact that the baryon density on a lattice is bounded from above by the ‘saturation density’, and the latter is of $O(1/a^d)$). The suppression in the sign problem in the saturation regime was also seen in the work of Ref. [27].

Another interesting fact is that $\langle \cos \theta \rangle$ drops from 1 at $\mu \approx m_\pi/2$ – as chiral perturbation theory predicts (see, for example, Ref. [4] and its references). Importantly, we point out that above $\mu/\sqrt{\lambda} \simeq 1.0$ the average sign is already very close to zero and so there is a severe sign problem there.

We now turn to study the way $\langle \cos \theta \rangle$ changes with N . Since the large N limit is the

thermodynamic limit in the EK theory, we expect the sign problem to become worse as N increases. This expectation is confirmed in Fig. 2 where we plot the average sign for $b = 10.00$ and for the gauge groups $SU(10)$, $SU(20)$, $SU(40)$ and $SU(60)$. We see that while there is no

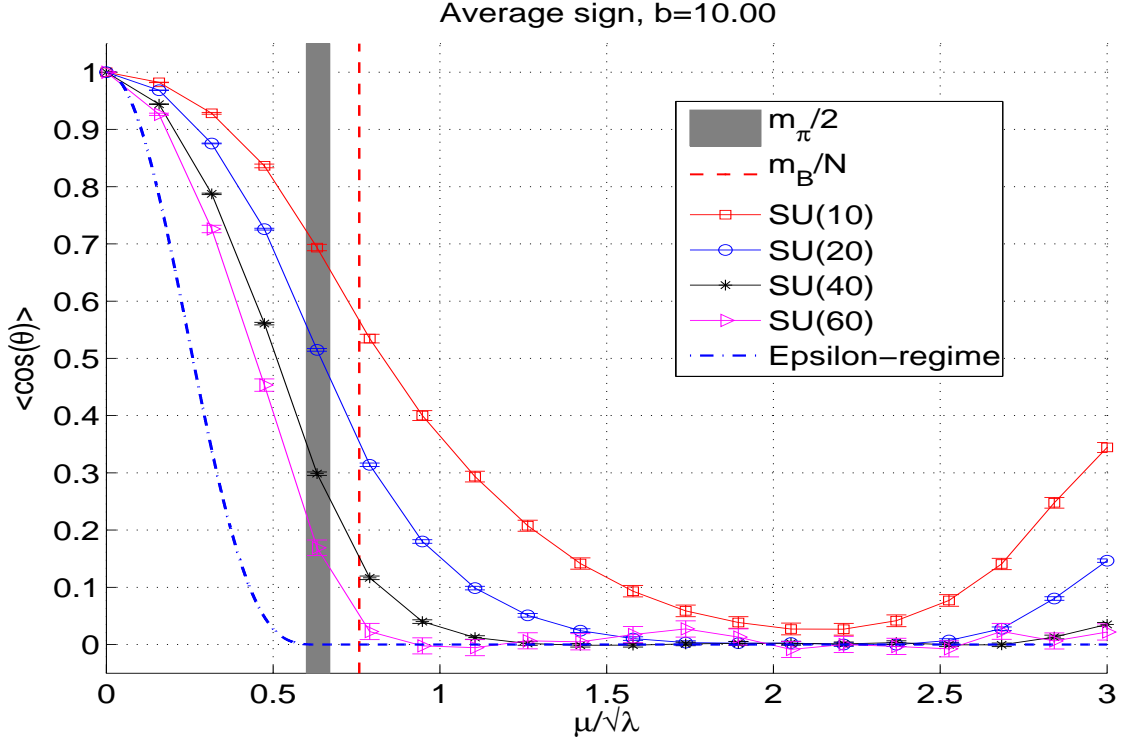


FIG. 2: Comparing the average sign of $SU(N)$ with $N = 10, 20, 40$ and 60 for $b = 10.00$. In a dash-dot(blue) line is the average sign of the epsilon regime.

serious sign problem in $SU(10)$ for any value of μ , for $SU(40)$ the average sign approaches zero at around $\mu/\sqrt{\lambda} \simeq 1.25$, and for $SU(60)$ the average sign is zero already at $\mu/\sqrt{\lambda} \simeq 0.75$. The way the average sign decreases with N is expected to be exponential if $\mu > m_\pi/2$. This can be easily argued if a different definition of an average sign is used (for example, see Ref. [4]). Because we do not use the definition of Ref. [4], we explicitly check how *our* definition for the sign changes with N . For that purpose we fix $\mu/\sqrt{\lambda} \simeq 0.95$ and measure $\langle \cos \theta \rangle$ for $b = 10.00$ and $N = 10, 20, 40$. The results are presented on a logarithmic plot in Fig. 3 and confirm that the sign drops approximately exponentially with N .

Before we proceed we wish to remark on the way the average sign behaves for $\mu < m_\pi/2$.

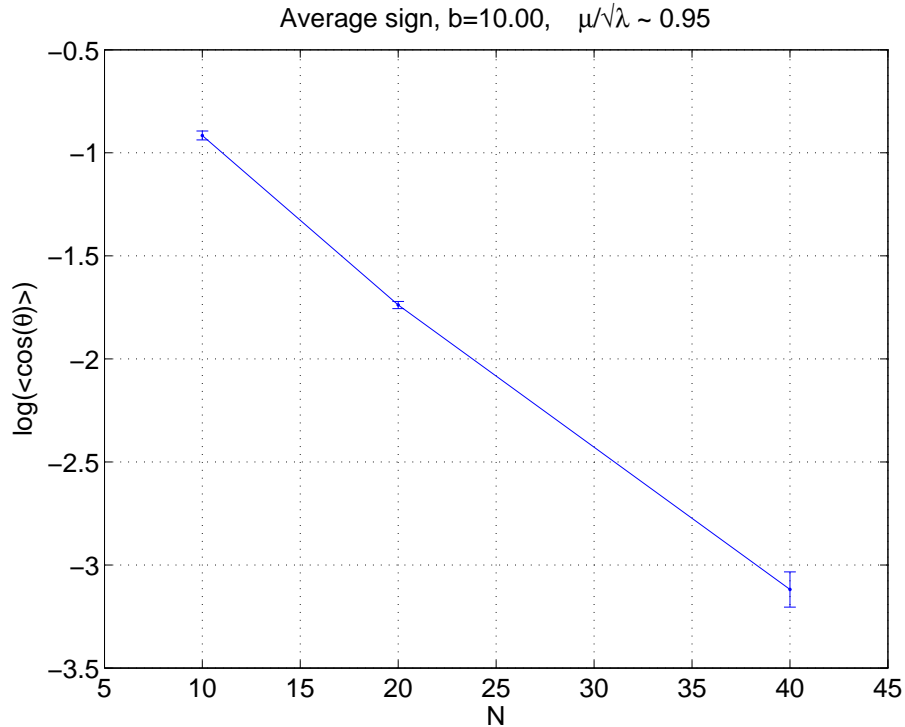


FIG. 3: A logarithmic plot of $\langle \cos(\theta) \rangle$ versus N at $b = 10.00$ and $\mu/\sqrt{\lambda} \simeq 0.95$.

Chiral perturbation theory gives different predictions for this behavior, depending on the value of the quark mass, the chemical potential and the volume. For example, in the thermodynamic limit, taken at fixed quark mass, the sign should freeze at one for all $\mu \leq m_\pi/2$ [28]. In the so-called ‘epsilon regime’, where the quark mass and μ are decreased when one takes the thermodynamic limit, the average sign approaches a smooth function of the variable $z \equiv (2\mu/m_\pi)^2$, that is equal to unity at $z = 0$ and to zero at $z = 1$. Therefore, interpreting the large- N limit as the thermodynamical limit of our system, we expect that the large- N limit of $\langle \cos \theta \rangle$ will be $O(1)$ for $z < 1$ and zero for $z \geq 1$. From Figs. (2)–(3) it is fairly clear that for $z > 1$ our results are consistent with this expectation. The situation for $\mu < m_\pi/2$ is less clear since we do not know whether our quark mass and the values of μ that we study are inside the epsilon regime or not (for that we would need to measure f_π). Nonetheless, the fact that the sign clearly drops with N suggests that we are either inside or close to the epsilon regime in that part of the phase diagram. Thus, as a guide to the eye we plot in Fig. 2 the average sign in the epsilon regime for our system. Here we assume that we are close enough to

the continuum limit, and so we plot the quenched averaged sign $\langle e^{4i\theta} \rangle_{\text{quenched}}$.⁸ The factor of 4 in the exponent reflects the fact that we use naive fermions in our numerical studies; in the continuum limit these fermions are four-fold doubled which means that our Dirac determinant $\det(D_{\text{lattice}})$ factorizes to $(\det D_{N_f=1})^4$, where $D_{N_f=1}$ is the Dirac operator of a single flavor theory in the continuum limit.

VII. TESTING Z_N AVERAGING.

We now proceed to test the Z_N averaging procedure by calculating the average sign of $(\det D)_Z$ for the same parameters presented in Fig. 2. We denote this quantity by $\langle \cos \theta \rangle_Z$, although we emphasize that what is measured is the sign of $(\det D)_Z$ and not the Z_N average of $\cos \theta$.

We present the results in Fig. 4 where we see that Z_N -averaging makes a dramatic difference: throughout the range of chemical potentials $\mu/\sqrt{\lambda} \in [0, 1.2]$ the Z_N -averaged quantity $(\det D)_Z$ is real and positive. In fact, the N dependence of $\langle \cos \theta \rangle_Z$ suggests that this positivity will persist until about $\mu/\sqrt{\lambda} \simeq 1.25$, a regime that includes, as a subset, all of the hadronic phase. This is most clearly seen by comparing Fig. 4 with Fig. 2 — there is a wide regime with $\mu > m_\pi/2$ where without Z_N averaging the sign is exponentially small but with Z_N averaging it is equal to one. Thus we see that, in that range, Z_N averaging solves the sign problem of our theory.

The absence of sign fluctuations below $\mu/\sqrt{\lambda} \simeq 1.25$ does not mean that there are no sign fluctuations for all μ . In fact, for $SU(40)$ there is a severe sign problem beyond the hadronic phase, in the range $\mu/\sqrt{\lambda} \in [1.8, 2.4]$.⁹ This is a real sign problem (i.e. it is not ‘just’ a silver-blaze problem) because it appears when observables start to be μ -dependent. Also note that *this* sign problem precedes the lattice saturation of the EK theory, where the sign fluctuations goes away again.

⁸ I.e. we set $p = 2$ in Eq. (48) of Ref. [4]

⁹ Our statistical errors in Fig. 4 are larger compared to those presented in Fig. 2 since we were able to calculate $\langle \cos \theta \rangle_Z$ for a fraction of our configurations in the $SU(40)$ case (recall that for each configuration we need to evaluate $\det D$ for each of the $40^2 = 1600$ terms in the sum in Eq. (4.1)). Thus, our resources allowed us to only do so for 5000 of the 105000 configurations.

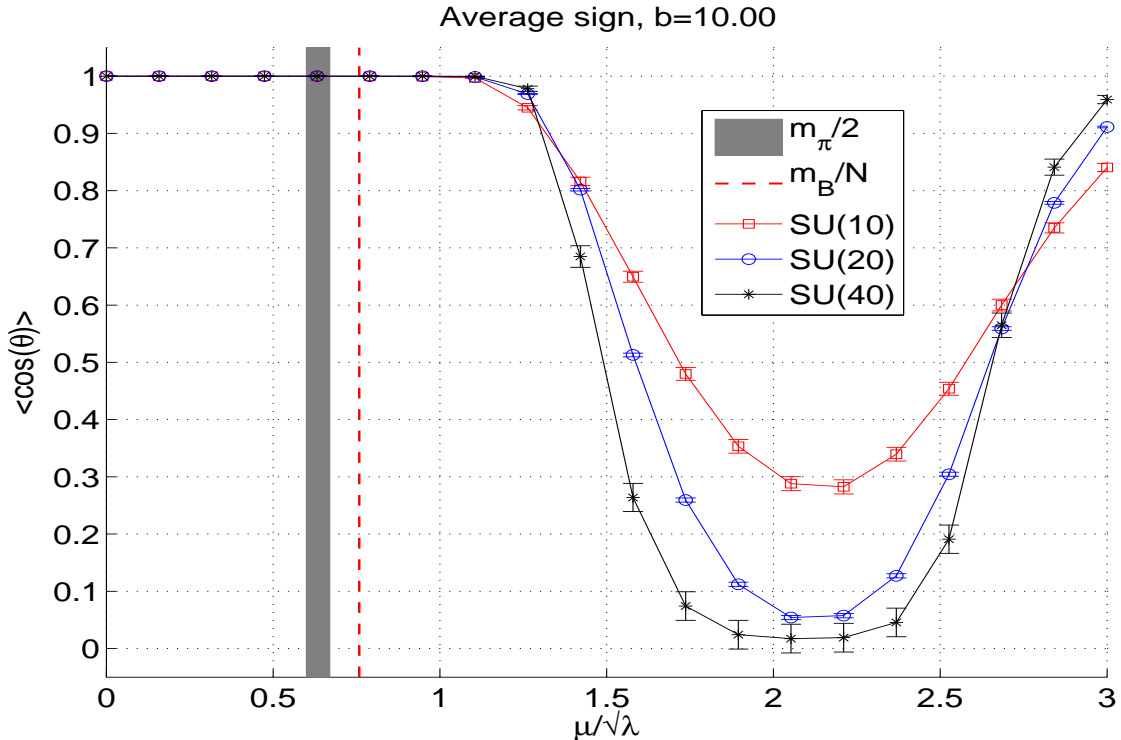


FIG. 4: The Z_N -averaged sign, $\langle \cos(\theta) \rangle_Z$, for $b = 10.00$ and $N = 10, 20, 40$.

What happens if we only perform a partial Z_N averaging (see discussion at the end of Section IV)? We present a comparison of the two type of averaging for $N = 40$ and $b = 10.00$ in Fig. 5. The fact that the two averaged signs are nearly the same (contrast their behavior with the non- Z_N -averaged sign in the figure) means that a partial Z_N averaging works almost as well as the full one, and indeed we shall use it when our resources cannot accomplish the latter. An interesting point appears when we compare the results of partial Z_N averaging for various values of N in Fig. 6. There, we see that, similarly to the full Z_N averaging case, the sign *grows* towards 1 for $\mu/\sqrt{\lambda} \lesssim 1.25$ and $\mu/\sqrt{\lambda} \gtrsim 2.75$. This means that in these ranges of μ , partial Z_N averaging removes the sign fluctuations from the averaging of $\det D$ in a way which is as good as the one provided by full Z_N averaging.

Let us now ask whether Z_N averaging actually improves the signal to noise ratio of physical observables. Since unquenched observables always involve the calculation of $\langle \det D \rangle$, we ask what is the improvement that Z_N averaging has to offer in the calculation of the latter (or

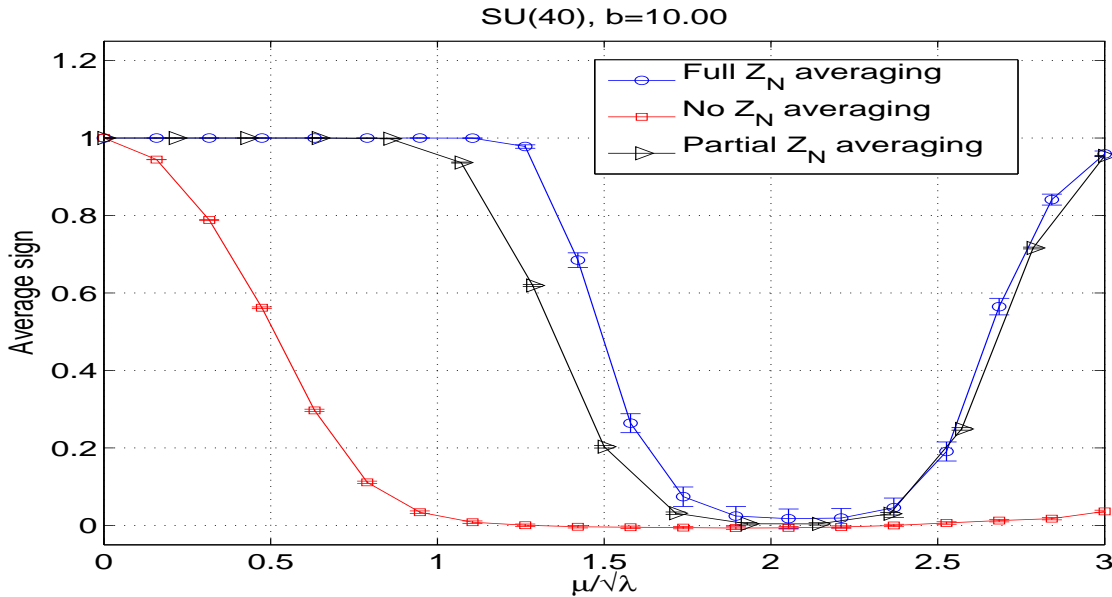


FIG. 5: The average sign with different versions of averaging. Here $b = 10.00$ and the gauge group is $SU(40)$.

more precisely in the calculation of the free energy $F \equiv \frac{1}{N} \log \langle \det D \rangle$.

To answer this question we check which of the following methods gives the smallest statistical error on F , provided we fix the computational effort.

- (1) No Z_N averaging. Here we average a set of M gauge configurations.
- (2) With partial Z_N averaging. Here we use a set of M/N gauge configurations. Recall that for given gauge configuration, we calculate the determinant N times (see Section IV).

We perform our check for $N = 40$, $M = 40000$, and $b = 10.0$ – a case where the sign problem can be relatively severe. The results of this check are given in Fig. 7. In the upper panel we show F , as obtained with both methods, and for convenience we show the corresponding average signs in the lower panel of the figure. A quick look at the figure shows that Z_N averaging can be useful. In fact, note that we do not show the results for F from method no. (1) when $\mu/\sqrt{\lambda} > 2.25$. This is because the severe sign fluctuations that appear in that method make the average of $\det D$ negative. In contrast, the average sign of method no. (2) is away from zero in the same regime and so $(\det D)_{\text{partial-Z}}$ is positive and real there. The most

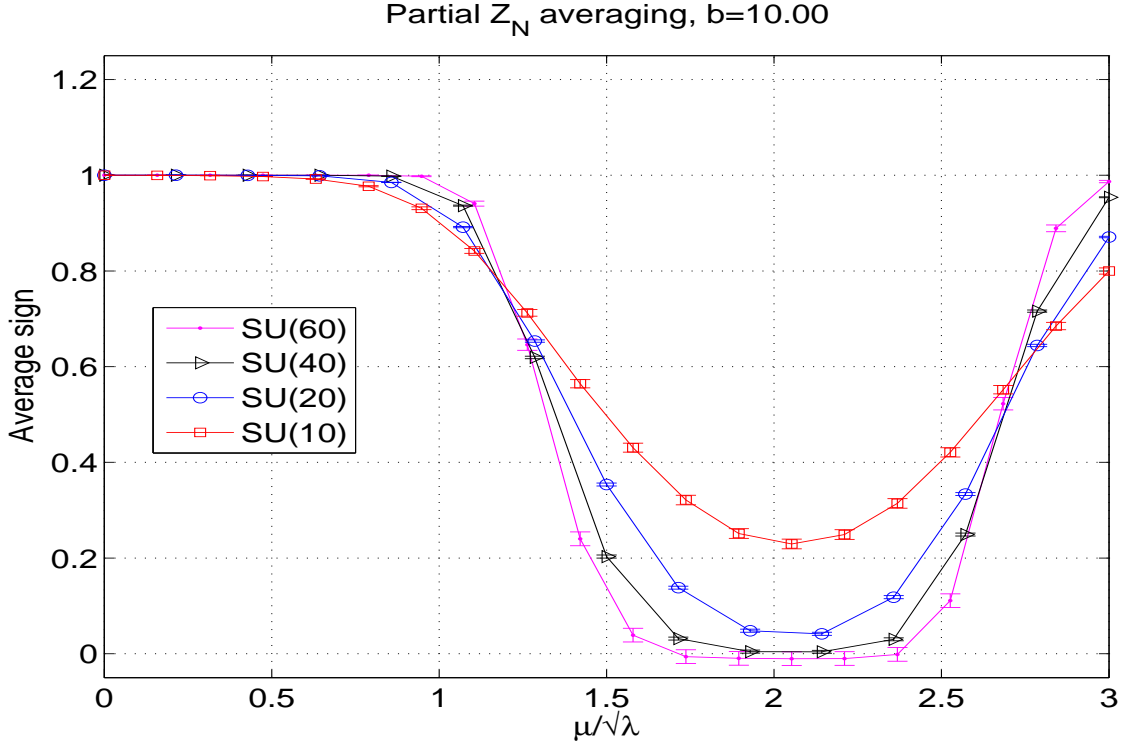


FIG. 6: The average sign with partial Z_N averaging. Here $b = 10.00$ and the gauge groups are $SU(10)$, $SU(20)$, $SU(40)$, and $SU(60)$.

important point, however, is that for $\mu/\sqrt{\lambda} \leq 1.25$ and $\mu/\sqrt{\lambda} \geq 2.75$, the sign is exponentially small in N with method no. (1) while it is increasing towards unity with method no. (2). Since the numerical cost of method no. (2) is linear in N , we see that it provides a gain which is exponential in N .¹⁰ To show the effect of the errors in the averages of $\det D$ on unquenched observables like $\langle \bar{\psi}\psi \rangle$, we plot the results obtained for $\langle \bar{\psi}\psi \rangle$ with the two methods in Fig. 8. Clearly Z_N averaging is useful here.

In the next section we show more results for F and $\langle \bar{\psi}\psi \rangle$. These were obtained with Z_N averaging and for much larger statistical samples than the ones we discuss above.

¹⁰ The fact that in method no. (2) one has less independent configurations might mean that its statistical error can be larger, but at sufficiently large- N and a moderately large number of configurations, the sign problem will always make method no. (2) preferable. This is already seen for $SU(40)$ in Fig. 7 in the range between $\mu/\sqrt{\lambda} \in [1, 1.25]$.

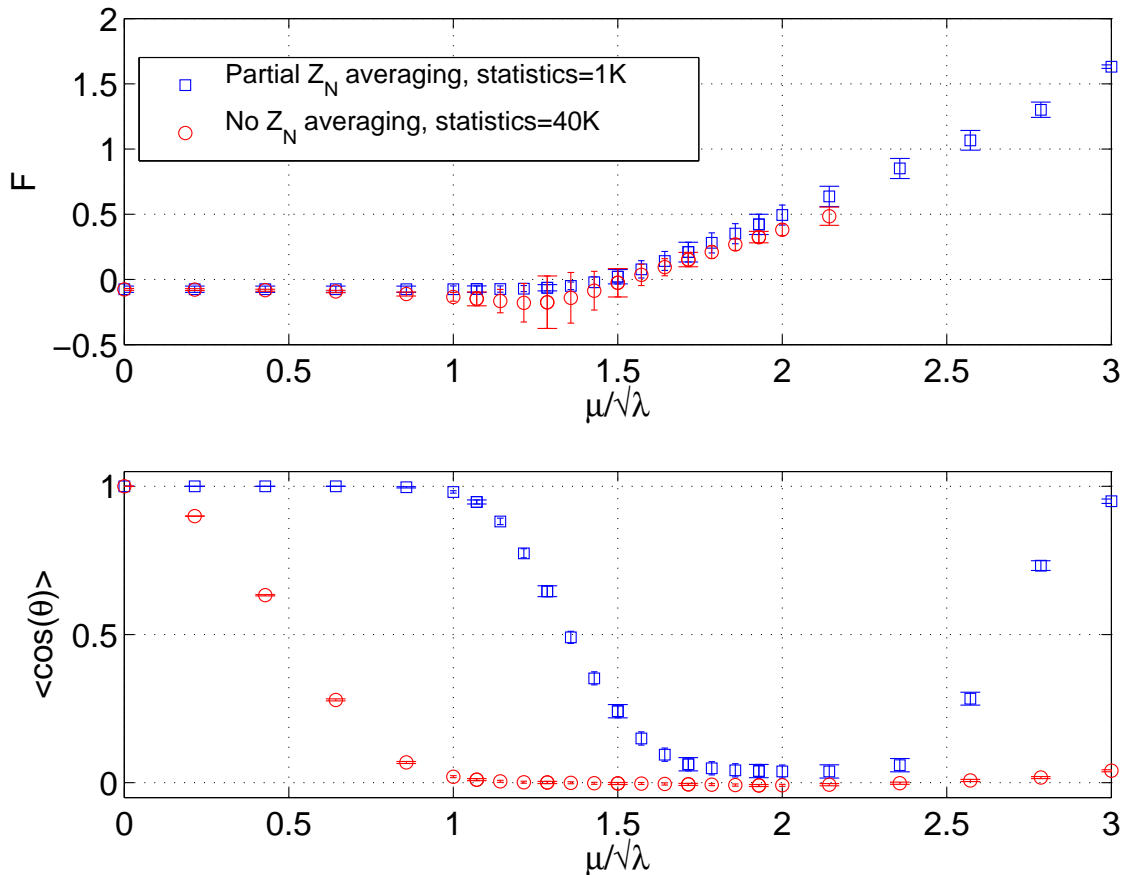


FIG. 7: A test of the efficiency of Z_N averaging for $SU(40)$ and $b = 10.0$. Squares (blue) show the result of method no. (2) while circles (red) those of method no. (1). In the upper panel we show F and in the lower one the average sign.

VIII. THE FREE ENERGY AND THE CHIRAL CONDENSATE

In this section we present several results of physical interest, beginning with the way the free energy F behaves as a function of μ . We calculated F using Z_N averaging and present the results for $b = 6.0, 10.0$ and $N = 10, 20$ in Fig. 9. Performing Z_N averaging for $N = 40$ was too challenging for our resources and so in that case we only used partial Z_N averaging. Also, while the $SU(40)$ results are similar to those of $SU(10)$ and $SU(20)$ for $\mu/\sqrt{\lambda} < 1.5$, the errors in the regime of the ‘true’ sign problem make the data not useful there – this is why we do not present the data for $b = 10.00$ in the regime $\mu/\sqrt{\lambda} \in [1.5, 2.75]$. Comparing this

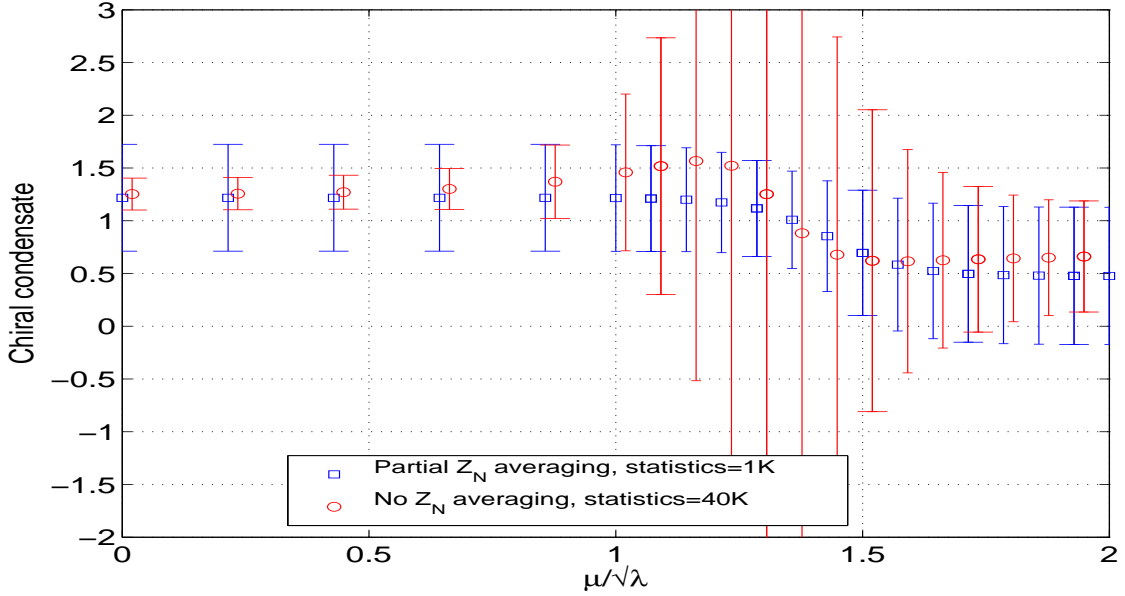


FIG. 8: A test of the efficiency of Z_N averaging for $SU(40)$ and $b = 10.00$ for the chiral condensate. Squares(blue) show the result of method no. (2) while circles(red) those of method no. (1). The data obtained with method no. (1) is slightly shifted on the x -axis, to distinguish it from the data of method no. (1).

figure to the upper panel of Fig. 7, we see that, beyond the hadronic phase, when the true sign problem is at its peak, even Z_N averaging does not help. This is reflected by the fact that while the smaller statistical sample used to produce Fig. 7 gave positive values of $\langle \det D \rangle$, the statistical sample we use in this section, which is 100 times larger, resulted in negative values of $\langle \det D \rangle$ in the same regime.

There are two additional important points to take away from Fig. 9. First, we see that the free energy is completely independent of μ throughout the hadronic phase, as we expect physically for $T = 0$. This is another way of seeing that the silver-blaze problem is absent from our calculation. Second, we see that F becomes $\simeq 2\mu$ for large value of μ . This is the lattice saturation we discussed above (see Eq. (6.2)).

To emphasize that the results in the preceding sections are truly unquenched we present the behavior of the quenched condensate $\langle \bar{\psi}\psi \rangle_{\text{quenched}}$ in Fig. 10. The sharp change in $\langle \bar{\psi}\psi \rangle_{\text{quenched}}$ at around $m_\pi/2$ is the same as seen in other quenched lattice calculations, and it is a non-

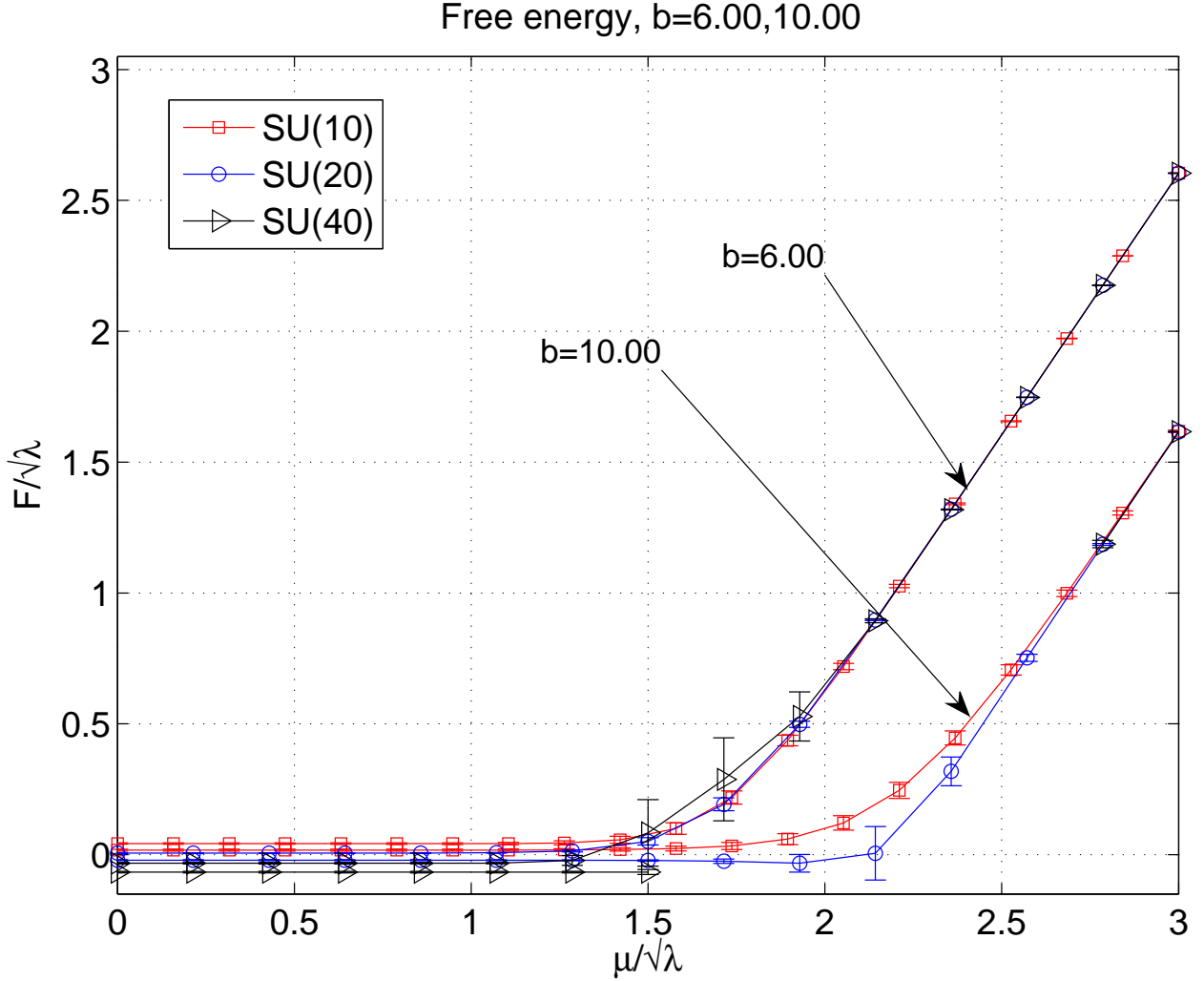


FIG. 9: The Z_N -averaged free energy density F_Z (see Eq. (3.14)) of $SU(10)$, $SU(20)$, and $SU(40)$ at $b = 6.0$ and 10.0 . The calculation for the $SU(40)$ case was done with partial Z_N -averaging. To guide the eye we connect the data with solid lines.

sensical result reflecting the mutilation that the quenched prescription causes to the gauge theory at nonzero μ . Comparing Fig. 10 to the plot of the free energy, Fig. 9, we see that the drop in the former happens at values of μ where the free energy is still independent of μ .

We attempted to use Z_N averaging and calculate the *unquenched* condensate, but for

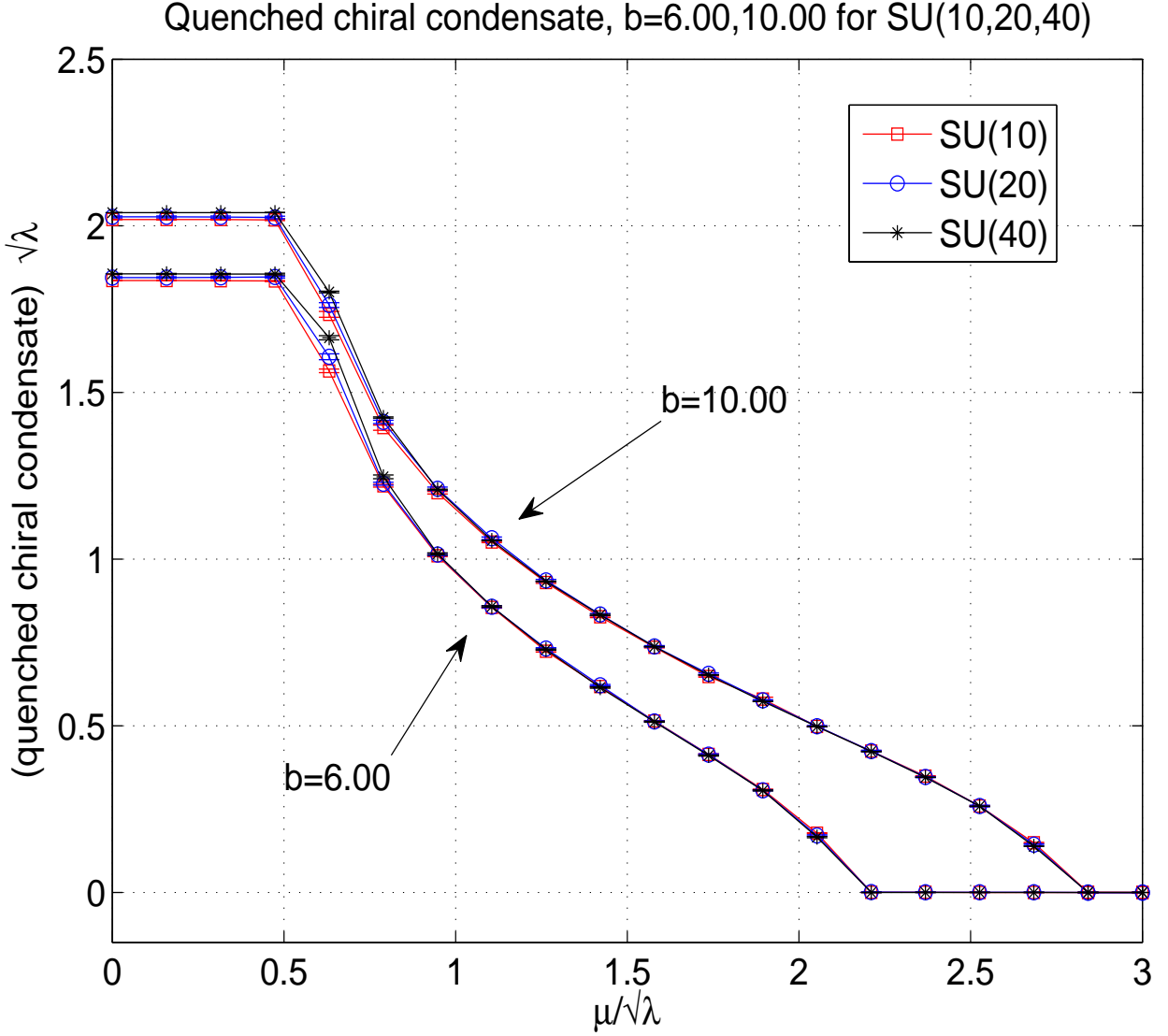


FIG. 10: The quenched quark condensate for $N = 10, 20, 40$ and $b = 6.00, 10.00$.

$SU(40)$ this proved too costly for our resources.¹¹ Instead, we calculated it using partial Z_N averaging (see Section IV). Let us now compare the quenched and unquenched condensates. We begin at $\mu = 0$, where we expect both condensates to be equal when $N = \infty$. We test this

¹¹ The bottle neck was not the generation of configurations, but rather the repeated calculation of the observables for each gauge configuration. For example, analyzing 10^4 measurements of $SU(40)$ for a single value of μ with Z_N averaging would take around 555 hours on a 2.66GHz CPU.

in Fig. 11 where we plot the difference $(\langle \bar{\psi}\psi \rangle_{\text{quenched}} - \langle \bar{\psi}\psi \rangle_{\text{unquenched}}) / N$ for the three lattice couplings 0.60, 6.0, 10.0 and versus $1/N$. As the figure shows, while the difference indeed goes

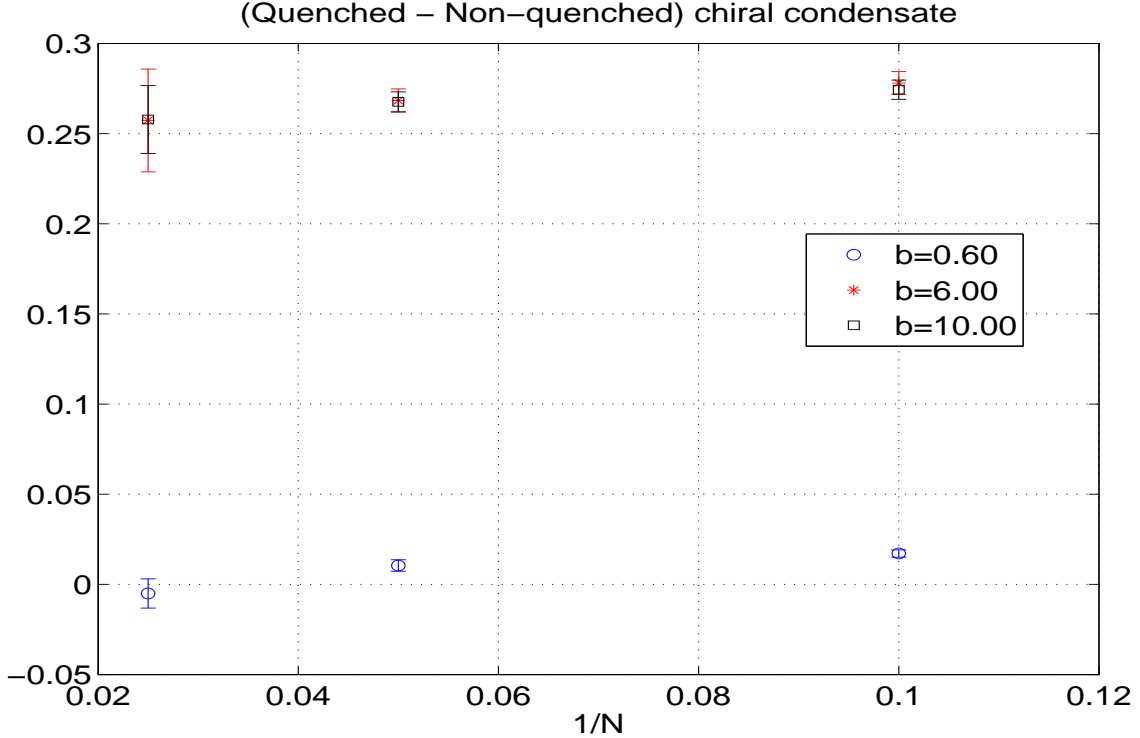


FIG. 11: The difference between the quenched and unquenched chiral condensate for $b = 0.60, 6.00, 10.00$ versus $1/N$ for $\mu = 0$.

to zero for $b = 0.60$, it does not seem to do so for $b = 6.0$ and 10.0 . We interpret this as resulting from working at too small values of N . Similar differences between quenched and unquenched averages at $\mu = 0$ were also reported for the overlap operator in this system [29]; it would be useful to understand this slow convergence to $N = \infty$, but this is beyond the goals of our current study.

We now turn to compare the quenched and unquenched condensates at $\mu \neq 0$. In this case, our discussion in Ref. [30] shows that the quenched approximation fails and that we should expect large $O(1)$ deviations (that do not go to zero at large N). While we explain this failure in Ref. [30] let us think about it from the point of view of the numerical calculation. If the quenched approximation was exact at large- N it would mean that the operators $\bar{\psi}\psi$ and $\det D$

are classical operators that obey large- N factorization since then we would have

$$\langle \bar{\psi}\psi \times \det D \rangle \stackrel{N \rightarrow \infty}{\cong} \langle \bar{\psi}\psi \rangle \times \langle \det D \rangle. \quad (8.1)$$

At nonzero μ we know that Eq. (8.1) fails because quenching fails — see the fictitious phase transition at $\mu = m_\pi/2$ observed in Fig. (10). Thus we expect correlations generated by the strong fluctuations that both $\bar{\psi}\psi$ and $\det D$ have within the complex plane. Put differently, the angles θ and α defined through Eqs. (3.18–3.19) now fully spread over the range $[-\pi, \pi)$ and can become correlated even when $N = \infty$. We will investigate this issue numerically in the next section.

A direct measure of such correlations is the way the difference between the quenched and unquenched chiral condensates behave as a function of μ . We already saw that at the values of N that we work with, the $\mu = 0$ condensates are different. This, however, we associated to significant $1/N$ corrections and distinguishing these from the $O(1)$ differences that we expect at nonzero μ , is hard to do unambiguously. Nevertheless, we attempt to do so by presenting in Fig. 12 the way the quenched and unquenched condensates, normalized by their $\mu = 0$ value, change with μ , for $b = 10.0$ and $N = 20$ and 40 .

There are a few useful observations we can make on Fig. 12. First, we see that the behaviors of the quenched and unquenched condensates as a function of μ strongly differ for chemical potentials that are above half the pion mass (denoted by the vertical magenta dashed line), as expected from chiral perturbation theory. Specifically, we see that despite the sharp change in $\langle \bar{\psi}\psi \rangle_{\text{quenched}}$ at $\mu \simeq m_\pi/2$, the physical unquenched condensate is unchanged throughout the hadronic phase and beyond. Second, we see that, within our statistical errors, the results for $N = 20$ and 40 are nearly on top of each other. Thus, combined with the theoretical expectations of Ref. [30], it does not seem likely that the differences between the quenched and unquenched averages that we see for $\mu \gtrsim m_\pi/2$ are $1/N$ effects. Finally, we see that the errors on the unquenched condensate greatly increase in the regime of the real ‘non-silver-blaze’ sign problem (see Fig. 3). All these facts are in agreement with physical expectations.

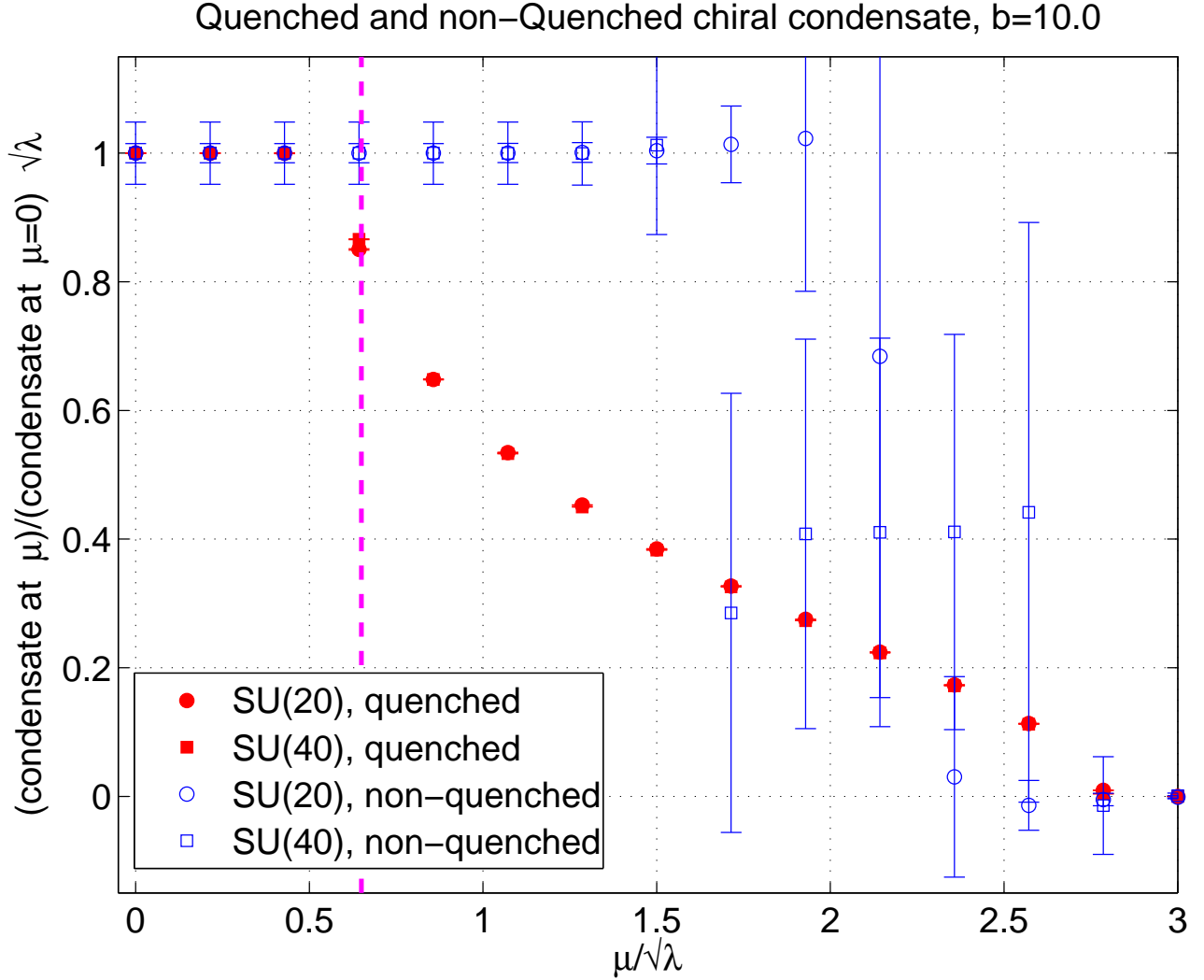


FIG. 12: The quenched and unquenched chiral condensate, normalized by their $\mu = 0$ value, versus μ . Here $b = 10.00$ and we present results for $N = 20, 40$. The vertical magenta dashed line denotes our estimate for half the pion mass (see Table I).

IX. DISTRIBUTIONS IN THE COMPLEX PLANE

This section has three goals. First we wish to examine the correlations between $\bar{\psi}\psi$ and $\det D$ that cause the failure of the quenched approximation. Second, we wish to see if our results for the distribution of θ (as defined by Eq. (3.18)) varies with μ as predicted by chiral perturbation theory [4]. In that reference, the authors showed that for $\mu < m_\pi/2$, θ is

distributed as a periodic Gaussian, while for $\mu > m_\pi/2$ the distribution becomes a periodic Lorentzian. Also, the widths of these distributions go to infinity in the thermodynamic limit (which in our case is the large- N limit). Third, we wish to see if the distribution of the eigenvalues of D in the complex plane is consistent with chiral perturbation theory.

We begin with analyzing the correlations between the phase α of $\bar{\psi}\psi$ and θ , and present these for $SU(20)$, $b = 6.0$, and different values of μ in Fig. 13. What we learn from the figure is that for most values of μ there is some correlation between α and θ . Especially, it seems that the fluctuations of α and θ are not small, and that for $\mu > m_\pi/2$, they spread in the range $[-\pi, \pi)$. We note that this, however, does not mean that they are strongly correlated since their joint probability distribution can still be approximately separable.

The probability distribution of θ itself is shown in Fig. 14 where we see that, as Ref. [4] anticipates, it is a periodic Gaussian for low values of μ . At larger values of μ it grows wider and flattens. We fitted $P(\theta)$ with the forms

$$P_G(\theta) \sim \sum_{n=-1000}^{1000} \exp\left[-(\theta + 2\pi n)^2 / \Delta\right] \quad (\text{periodic Gaussian}), \quad (9.1)$$

$$P_L(\theta) \sim 1/[\Delta - \cos\theta] \quad (\text{periodic Lorentzian}). \quad (9.2)$$

We present the resulting parameters of the fits in Table II. The statistical error on the fit parameters represents the one-sigma error from the fit, as well as the differences between fits done for histograms generated by cutting the full statistical sample into $N_{\text{bin}} = 15, 25$ and 35 bins. The different values of the χ^2 in the table represent this dependence on N_{bin} . Our fits were uncorrelated, and changing N_{bin} is the way we check for the correlation of the different bins in the histogram.

From the table we see that while the periodic Gaussian can be fitted to the data for low and high values of μ , the Lorentzian form cannot. At $\mu \simeq 1.7\sqrt{\lambda}$ the Lorentzian becomes consistent with the data, but at that point the histogram is so flat that both the Gaussian and the Lorentzian can be good fits. Note also that the values of χ^2 are not too small, but looking at the plots they seem to reflect a general scatter of the data around the curve and so are likely to come from an underestimate of the statistical error.

Let us now ask how Fig. 13 and Fig. 14 change when we increase N . The results for $SU(40)$ are given in Figs. 15-16 and we see that increasing N makes the distribution of both θ and α

$\mu/\sqrt{\lambda}$	Gauge group	Gaussian fit		Lorentzian fit	
		Δ	χ^2/dof	Δ	χ^2/dof
0.31579	$SU(20)$	0.71(3)	1.6 – 2.7	No fit	
	$SU(40)$	1.17(1)	0.8 – 1.6	No fit	
0.78947	$SU(20)$	6.5(1)	1.8 – 2.5	No fit	
	$SU(40)$	11.5(5)	0.9 – 1.3	9.0(7)	0.7 – 1.0
1.7368	$SU(20)$	17(2)	1.8 – 3.1	40(20)	1.8 – 3.0
	$SU(40)$	18(3)	1.2 – 1.5	50(30)	1.6 – 1.5
2.8421	$SU(20)$	2.84(4)	1.0 – 2.8	No fit	
	$SU(40)$	4.65(5)	0.6 – 0.9	No fit	

TABLE II: Results of fits to the histograms in θ (see text).

more spread out. The corresponding fitting results to the distribution $P(\theta)$ in this case are also presented in the Table II.

It is hard to conclude from the figures how the correlations between θ and α changes with N . Nevertheless, the widening of the histograms in Fig. 16 compared to Fig. 14 is qualitatively consistent with Ref. [4] if we interpret the large- N limit as the thermodynamical limit. More accurate studies are required to pinpoint the nature of the correlation between $\bar{\psi}\psi$ and $\det D$ (the absolute values of $\bar{\psi}\psi$ and $\det D$ may play a role also). Probably the best indicator for this is the connected correlation function between these operators, which is nothing but the difference between the unquenched $\langle\bar{\psi}\psi\rangle$ and $\langle\bar{\psi}\psi\rangle_{\text{quenched}}$. As we mentioned in Section VIII, this difference is significantly nonzero and independent of N for $\mu > m_\pi/2$.

We note in passing that we see that the χ^2 for $SU(40)$ cases are lower than for $SU(20)$ and this may reflect the presence of significant $1/N$ corrections that are required to make the the fitting ansatz in Eqs. 9.1–9.2 consistent with our data. Also, we see that, as predicted by chiral perturbation theory, the Lorentzian is consistent with our data at $\mu \simeq 0.8\sqrt{\lambda}$. This should only be seen as partial evidence to support these predictions since for the same values of μ , the Gaussian is also consistent with our data, and because for $SU(20)$ it is only the Gaussian that provides an acceptable fit at that value of μ . Finally we note the way Δ depends on N is

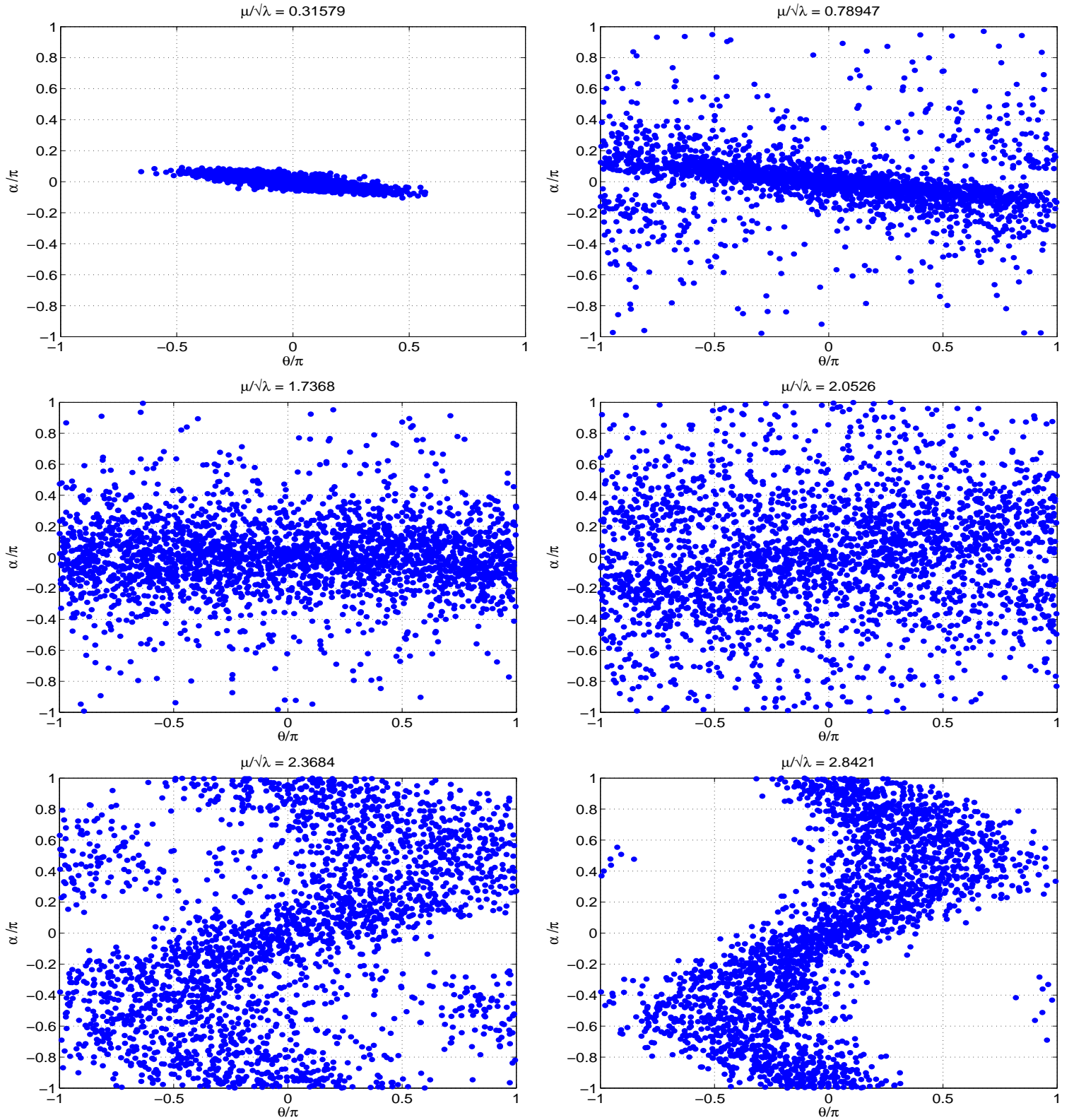


FIG. 13: The correlations between α and θ (see text) for $SU(20)$, $b = 6.0$, and various values of μ .

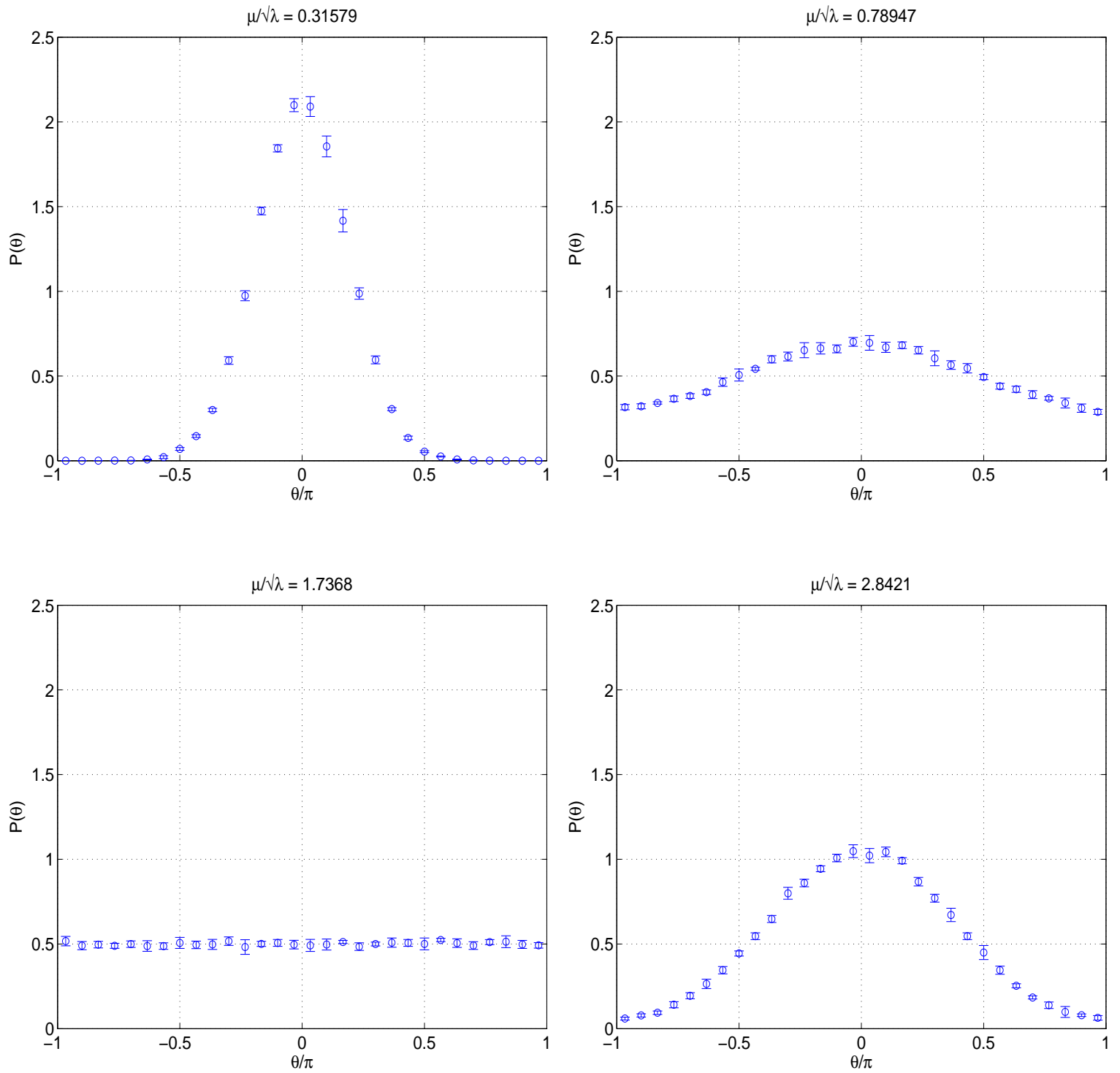


FIG. 14: The probability density of θ for $SU(20)$, $b = 6.0$ and various values of μ . The solid curves are the Gaussian fits (see Table II).

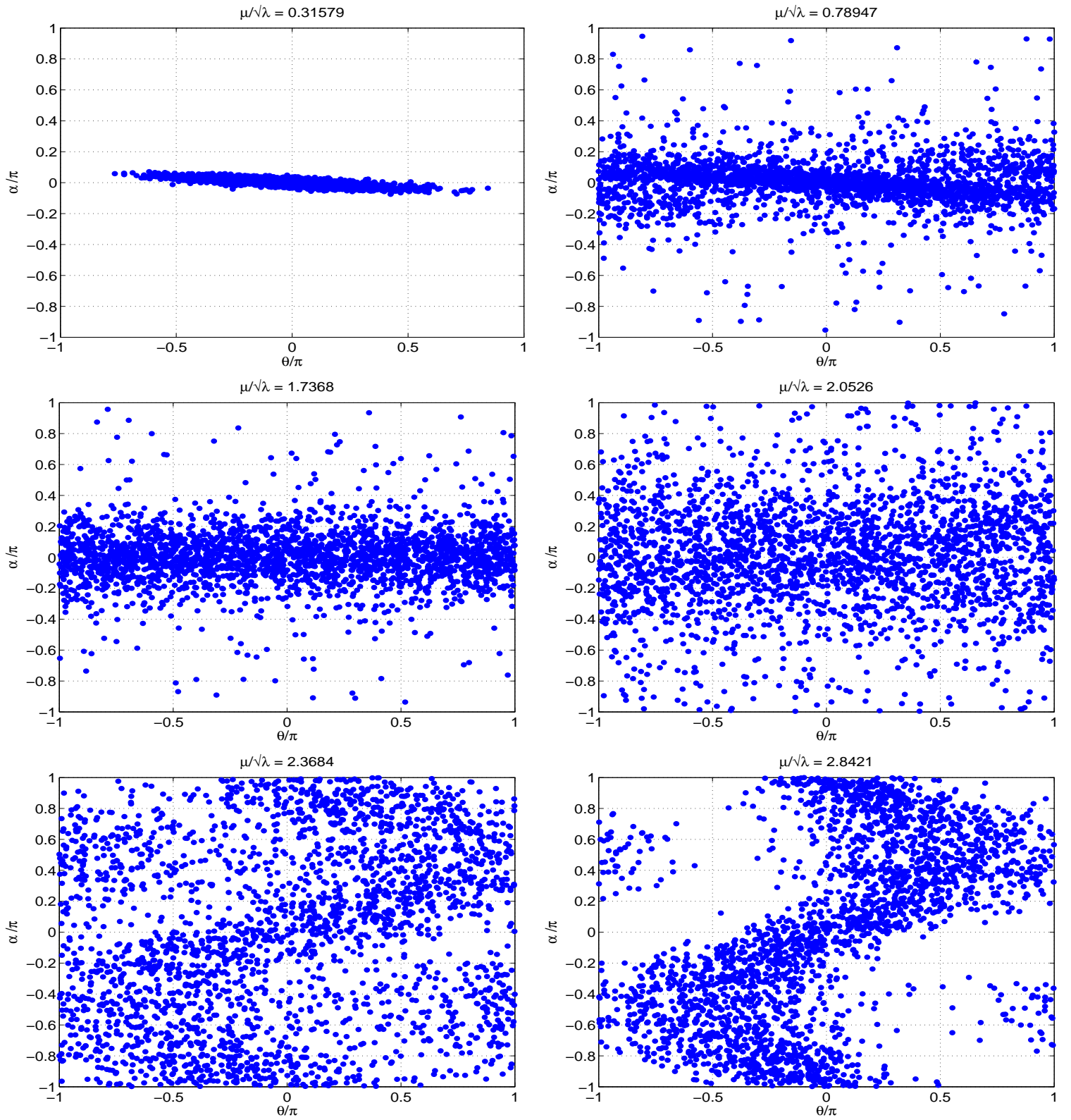


FIG. 15: Same as Fig. 13, but for $SU(40)$.

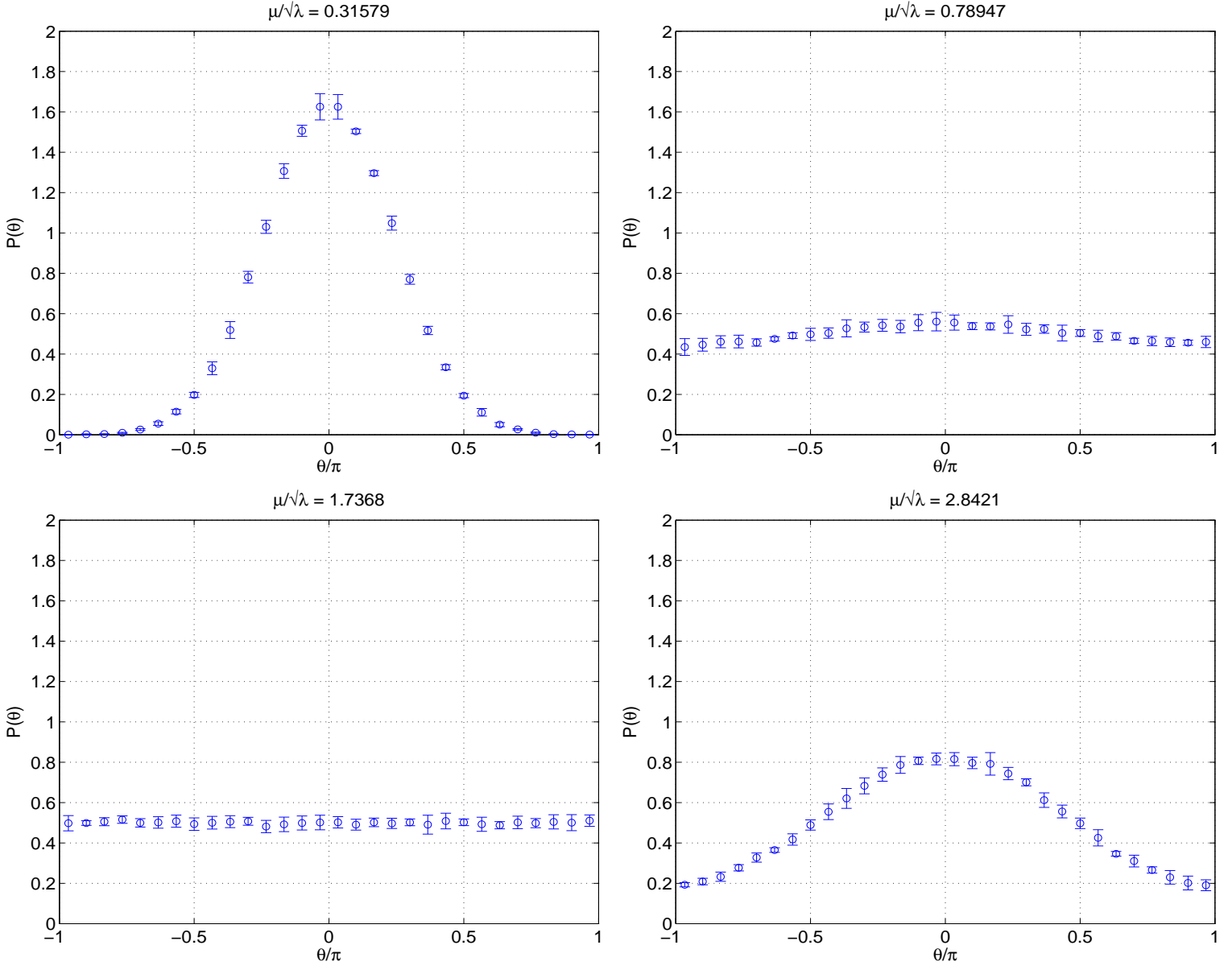


FIG. 16: The same as Fig. 14, but for $SU(40)$. The only panel that includes both the Gaussian and the Lorentzian fit is that of $\mu \simeq 0.79\sqrt{\lambda}$. The Gaussian curve is a solid line (blue), and the Lorentzian is the dashed (red). It is clear that both are very close to each other.

expected to be linear for the Gaussian case (see Ref. [4], but this is only partially consistent with what we see in Table II; this is expected to happen only for $\mu \simeq 0.32\sqrt{\lambda} < m_\pi/2$, but there we see that $\Delta_{SU(40)}/\Delta_{SU(20)} = 1.65(7)$ instead of 2. In the case of $\mu \simeq 2.8\sqrt{\lambda}$, where

$P(\theta)$ is clearly Gaussian and not a Lorentzian, we see that $\Delta_{SU(40)}/\Delta_{SU(20)} = 1.64(3)$. We do not fully understand these results which actually correspond to $\Delta_{SU(N)} \sim N^{0.71(3)-0.72(6)}$. They may reflect significant $1/N$ corrections in the $SU(20)$ case.

We end this section by presenting the way the eigenvalues of D are scattered in the complex plane. According to chiral perturbation theory, when $\mu < m_\pi/2$, the bare quark mass m is outside the support of the eigenvalue distribution, while for $\mu > m_\pi/2$ it is within it. This is confirmed in Fig. 17 where we show the eigenvalue scatter of 50 gauge configurations for $SU(40)$ and $b = 6.00$. We present the cases of $\mu/\sqrt{\lambda} = 0.31579, 0.60, 0.78947$ which are below, close to, and above $\frac{1}{2}m_\pi/\sqrt{\lambda}$. Also, the cases of $\mu/\sqrt{\lambda} \simeq 0.31579, 0.78947$ correspond to the two upper panels of Figs. 15–16. Recall that in our current work we fix the quark mass to be $m/\sqrt{\lambda} = 1/\sqrt{\pi} \simeq 0.5642$ (see Eq. (3.7)).

X. SUMMARY AND CONCLUSIONS

In this paper we studied the sign problem of the euclidean path integral of large- N QCD at nonzero chemical potential μ . To do so we used the Eguchi-Kawai (EK) equivalence which allows us to approach the problem via the volume reduced version of theory. For reasons of computational cost we focused on the two dimensional case in this paper. Extensions to four dimensions are straight forward and we discuss them below.

We used lattice Monte-Carlo simulations to explore the sign problem numerically and did so for three lattice spacing, and for $SU(N)$ gauge groups with $N \leq 60$. We measured the average sign of $\det D$, and saw that it decreases to zero when $\mu \simeq m_\pi/2$, but then rises back to 1 when the lattice site is saturated with quarks.

We proposed a way to suppress the sign fluctuations in the hadronic phase which amounts to replacing the pure-gauge average of $\det D$, by an average over a real and positive quantity. We denote the latter by $(\det D)_Z$, and it is the average of $\det D$ over a set of gauge configurations that are related by Z_N center transformations. We call this method ‘ Z_N -averaging’ (see also [8]) and we test it numerically. We find it to be successful and that, in the large- N volume-reduced system, the average sign of $(\det D)_Z$ is 1 for a wide range of μ that includes all the hadronic phase. Thus, this method removes the sign fluctuations from the hadronic

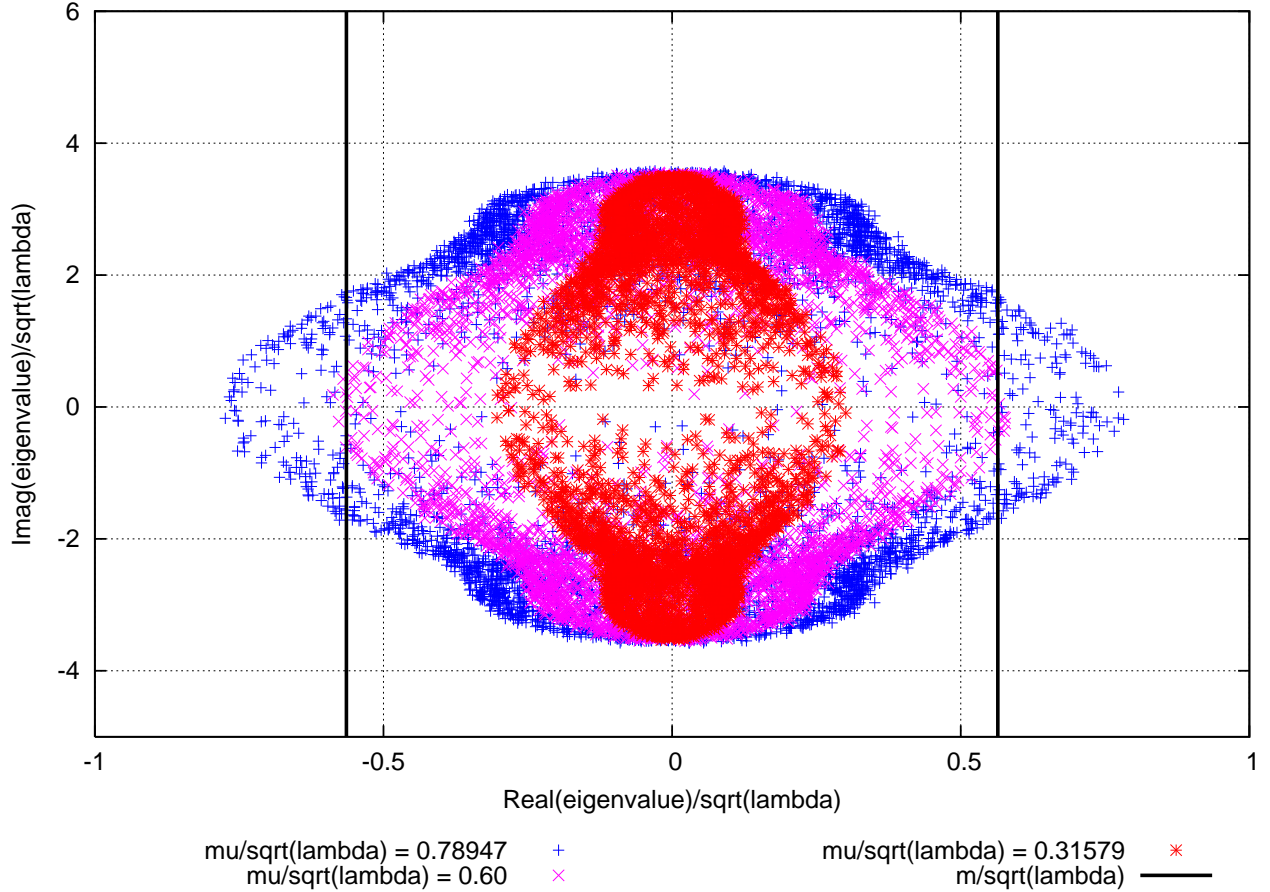


FIG. 17: The scatter in the complex plane of the eigenvalues of D . Here $b = 6.00$ and the gauge group was $SU(40)$.

phase. The computational cost of Z_N averaging grows linearly in N , and this means it provides an exponential gain in calculating the average of $\det D$, since the computational cost of overcoming the sign fluctuations involved in such an average by brute force grows exponentially in N . This means that Z_N averaging solves the silver blaze problem in our volume-reduced large- N theory.

Z_N -averaging also identifies the regime in μ where the true, non-silver-blaze, sign problem of the large- N reduced theory is most severe. The latter happens beyond the hadronic phase, just before the saturation regime. We identified the saturation regime also in measurements of the free energy, which becomes linear in μ in that regime. Our measurements of the free energy and of the chiral condensate are unquenched and as anticipated physically, we see

that they show μ -independence throughout the hadronic phase. Our measurements of the *quenched* chiral condensate serve to contrast this since they show that $\langle \bar{\psi}\psi \rangle_{\text{quenched}}$ changes at around $\mu \simeq m_\pi/2$, where nothing happens to the free energy and to the physical unquenched condensate. This reflects the breakdown of the quenched approximation.

In an attempt to numerically understand the failure of the quenched approximation mentioned above, we analyzed the way the operators $\bar{\psi}\psi$ and $\det D$ are correlated with each other for different values μ . Specifically, we checked whether their correlations is mostly due to a correlation between the phases of the operators, but were not able to unambiguously conclude if this is the case or not. Instead, we directly calculated the connected correlation of $\bar{\psi}\psi$ and $\det D$. This correlation is nothing but the difference between the quenched and unquenched chiral condensates. We saw that this difference becomes large for $\mu \gtrsim m_\pi/2$, and that it does not go down with increasing N . This means that the failure of the quenched prescription can be thought of as the breakdown of large- N factorization. It would be useful to understand this breakdown from a physical point of view rather than a numerical one. It will also be useful to understand our results for the difference between the quenched and unquenched condensates at $\mu = 0$ and verify that they go away at $N \rightarrow \infty$ by performing simulations for large values of N .

We also measured the way the phase of $\det D$ is distributed as a function of N and μ , and saw that, in agreement with chiral perturbation theory (see Ref. [4]), these distributions are Gaussian for $\mu < m_\pi/2$ and become extended when μ increases beyond that. The width of these distributions increases towards the thermodynamical limit of $N \rightarrow \infty$. At the quantitative level, our results support the predictions of Ref. [4] only partially, but this may be due to $1/N$ effects. Finally, we confirmed that when $\mu > m_\pi/2$ the quark mass m enters the support of the density of eigenvalues of D .

The analysis we presented here can in principle be repeated for four dimensions but this will require more work. In particular, in $4d$, the straight forward EK theory is not equivalent to large- N QCD (even in the hadronic phase) and other prescriptions, like those suggested in Refs [12] and [13] (and studied numerically in Refs. [14] and [15]), are needed to overcome this issue. Once this is done, and one has a set of pure-gauge field configurations in hand, then the methods of this paper can be used with a modest increase in computational effort.

Specifically, the only change is that the dimension of the Dirac matrix D is doubled relative to the two-dimensional case. We therefore estimate that future $4d$ studies of the issues we explore in this work are feasible.

Finally, we proposed that Z_N averaging solves the silver blaze problem when the contribution to the Dirac operator determinant from baryonic worldlines (or Polyakov loops whose winding number is a multiple of N) is suppressed on a configuration-by-configuration basis (for an explanation of this see Section VB). In the current paper we see numerically that in $1+1$ dimensions such suppression indeed takes place in the large- N volume-reduced version of the QCD, but we do not know if this is also the case for physical (four dimensional and 3-color) QCD. More precisely, in Section VB we discussed how such a suppression will *not* happen at $T \rightarrow 0$ since, in that limit, a configuration with k baryonic worldlines will most likely be only moderately suppressed by the Boltzmann factor of $e^{-kNm_\pi/(2T)}$. We argued, however, that there may be a region of $T > 0$ where, instead, these worldlines might be suppressed and where Z_N averaging would work. This ‘golden region’ is the analog of the ‘golden window’ in the studies of baryon correlation functions [26], where one searches for optimized baryonic wave functions whose noise couples very little to pion systems. Therefore it seems interesting to attempt Z_N averaging in physical QCD (with light quarks) and try and locate this golden region.

Acknowledgments

For useful discussions and correspondences I thank A. Alexandru, S. Chandrasekharan, Ph. d. Forcrand, R. Narayanan, K. F. Liu, Weonjong Lee, M. P. Lombardo, S. R. Sharpe, K. Splittorff, J. Verbaarschot, and L. G. Yaffe. I wish to thank G. Aarts and S. Chandrasekharan for organizing the interesting “Sign Problems and Complex Actions” workshop at the ECT*, the ECT* for its kind hospitality, and the KITP-Beijing, where part of this study was completed, for its support. Finally, for constant encouragement and support I thank Sarit Goren. This work was supported by the U.S. Department of Energy under Grant No. DE-FG02-96ER40956 and also in part by the Project of Knowledge Innovation Program

(PKIP) of Chinese Academy of Sciences, Grant No. KJCX2.YW.W10.

- [1] Ph. de Forcrand, arXiv:0807.0860 [hep-lat].
- [2] Ph. de Forcrand, Plenary talk at Lattice 2009.
- [3] T. D. Cohen, Phys. Rev. Lett. **91**, 222001 (2003) [arXiv:hep-ph/0307089].
- [4] M. P. Lombardo, K. Splittorff and J. J. M. Verbaarschot, arXiv:0904.2122 [hep-lat].
- [5] G. Aarts, Phys. Rev. Lett. **102**, 131601 (2009) [arXiv:0810.2089 [hep-lat]].
- [6] S. Chandrasekharan, arXiv:0910.5736 [hep-lat].
- [7] C. Gattringer and L. Liptak, arXiv:0906.1088 [hep-lat].
- [8] A. Hasenfratz and D. Toussaint, Nucl. Phys. B **371**, 539 (1992). M. G. Alford, S. Chandrasekharan, J. Cox and U. J. Wiese, Nucl. Phys. B **602** (2001) 61 [arXiv:hep-lat/0101012]. G. Aarts, O. Kaczmarek, F. Karsch and I. O. Stamatescu, Nucl. Phys. Proc. Suppl. **106**, 456 (2002) [arXiv:hep-lat/0110145]. T. T. Takahashi, arXiv:0807.0864 [hep-lat]. Y. Sasai, A. Nakamura and T. Takaishi, Nucl. Phys. Proc. Suppl. **129**, 539 (2004) [arXiv:hep-lat/0310046]. B. Bringoltz, talk at the “Sign Problems and Complex Actions” workshop at the ECT*, Trento, Italy, March 2009. S. Chandrasekharan, talk at the “Sign Problems and Complex Actions” workshop at the ECT*, Trento, Italy, March 2009.
- [9] T. Eguchi and H. Kawai, Phys. Rev. Lett. **48**, 1063 (1982).
- [10] G. Bhanot, U. M. Heller and H. Neuberger, Phys. Lett. B **113**, 47 (1982).
- [11] V. A. Kazakov and A. A. Migdal, Phys. Lett. B **116**, 423 (1982).
- [12] M. Unsal and L. G. Yaffe, Phys. Rev. D **78**, 065035 (2008) [arXiv:0803.0344 [hep-th]].
- [13] P. Kovtun, M. Unsal and L. G. Yaffe, JHEP **0706**, 019 (2007) [arXiv:hep-th/0702021].
- [14] B. Bringoltz and S. R. Sharpe, arXiv:0906.3538 [hep-lat].
- [15] A. Hietanen and R. Narayanan, arXiv:0911.2449 [hep-lat].
- [16] B. Bringoltz, Phys. Rev. D **79**, 105021 (2009) [arXiv:0811.4141 [hep-lat]].
- [17] B. Bringoltz, Phys. Rev. D **79**, 125006 (2009) [arXiv:0901.4035 [hep-lat]].
- [18] V. Schon and M. Thies, Phys. Rev. D **62**, 096002 (2000) [arXiv:hep-th/0003195].
arXiv:hep-th/0008175.

- [19] L. L. Salcedo, S. Levit and J. W. Negele, Nucl. Phys. B **361**, 585 (1991).
- [20] J. Kiskis, R. Narayanan and H. Neuberger, Phys. Rev. D **66**, 025019 (2002) [arXiv:hep-lat/0203005].
- [21] K. Fabricius and O. Haan, Phys. Lett. **143B**, 459 (1984).
- [22] D. J. Gross and Y. Kitazawa, Nucl. Phys. B **206**, 440 (1982).
- [23] R. Narayanan and H. Neuberger, Phys. Lett. B **616**, 76 (2005) [arXiv:hep-lat/0503033]. A. Hietanen, R. Narayanan, R. Patel and C. Prays, Phys. Lett. B **674**, 80 (2009) [arXiv:0901.3752 [hep-lat]].
- [24] S. Kratochvila, Phd thesis, “Extracting physics from weak signals in lattice gauge theory,” 2006.
- [25] X. f. Meng, A. Li, A. Alexandru and K. F. Liu, PoS **LATTICE2008** (2008) 032 [arXiv:0811.2112 [hep-lat]].
- [26] W. Detmold, Multi-hadron systems, plenary talk given at the XXVII International Symposium on Lattice Field Theory, Beijing, China (July 2009), to be published in the proceedings.
- [27] M. Fromm and P. de Forcrand, arXiv:0811.1931 [hep-lat].
- [28] K. Splittorff and J. J. M. Verbaarschot, Phys. Rev. D **77**, 014514 (2008) [arXiv:0709.2218 [hep-lat]].
- [29] R. Narayanan, private communications.
- [30] Barak Bringoltz and L. G. Yaffe, in preparation.